

Tunable anyonic permeability across \mathbb{Z}_2 spin liquid junctions

Sayak Bhattacharjee,^{1,*} Soumya Sur,^{2,†} and Adhip Agarwala^{2,‡}

¹*Department of Physics, Stanford University, Stanford, California 94305, USA*

²*Department of Physics, Indian Institute of Technology Kanpur, Kalyanpur, UP 208016, India*

We introduce two classes of junctions in a toric code, a prototypical model of a \mathbb{Z}_2 quantum spin liquid, and study the nature of anyonic transport across them mediated by Zeeman fields. In the first class of junctions, termed potential barrier junctions, the charges sense effective static potentials and a change in the band mass. In a particular realization, while the junction is completely transparent to the electric charge, magnetic charge transmission is allowed only after a critical field strength. In the second class of junctions we stitch two toric codes with operators which do not commute at the junction. We show that the anyonic transmission gets tuned by effective pseudospin fluctuations at the junction. Using exact analytical mappings and numerical simulations, we compute charge-specific transmission probabilities. Our work, apart from uncovering the rich physical mechanisms at play in such junctions, can motivate experimental work to engineer defect structures in topologically ordered systems for tunable transport of anyonic particles.

Introduction: Controlled anyonic scattering has been at the forefront of quantum technology research in a wide range of systems—especially in the context of the fractional quantum Hall effect [1–10] and quantum spin liquids [11–19] in solid-state devices as well as cold-atom simulators [20–27]. While the study of disorder [28–34] and defects [35–41] in \mathbb{Z}_2 spin liquids has been extensively done, the study of junctions of topologically ordered structures and their role in anyonic transport has been little explored [42–45]. Although junctions have played a defining role in tuning electronic transport, the development of governing principles and/or concrete models for anyonic equivalents is still nascent. In this work, we fill this gap by introducing two classes of junctions between otherwise translationally uniform two-dimensional \mathbb{Z}_2 toric codes (TC) [46], the paradigmatic model for a \mathbb{Z}_2 spin liquid [47]. The ground state(s) of the TC exhibit topological order [48] whose low-energy excitations are Abelian anyons [49–52]—bosonic electric (e) and magnetic charges (m) and their fermionic bound state, the dyon (ψ). Our focus on this work will be on tuning the transmission probabilities of e and m charges by distinct physical mechanisms dependent on the nature of the two classes of junctions we discuss: (1) the potential barrier junction and (2) the phase junction.

In the *potential barrier junction* we uniformly modify the TC couplings in a region sandwiched between two other regions. We consider the TC defined on a square lattice [46] with two sets of stabilizers—star (A_v^z) and plaquette (B_p^x), associated with a vertex v and plaquette p , respectively—each constructed using spin-1/2 (σ) operators of strength J defined on the links, and with a Hamiltonian,

$$H_{\text{TC}} = -J \sum_v A_v^z - J \sum_p B_p^x. \quad (1)$$

* equally contributed; sayakbhattacharjee@stanford.edu

† equally contributed; ssoumya@iitk.ac.in

‡ adhip@iitk.ac.in

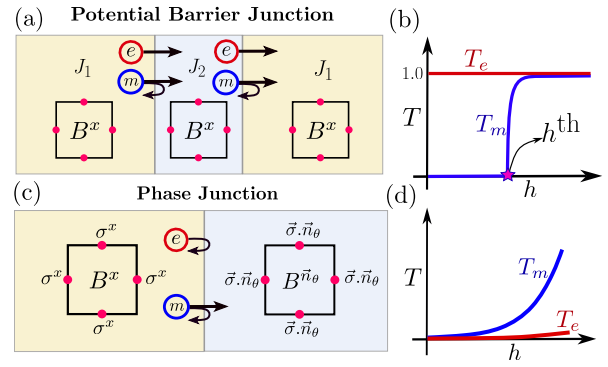


FIG. 1. **Two classes of toric code junctions:** Schematic figures of (a) a *potential barrier* J_1 - J_2 junction (Eq. 2) and (c) the *phase junction* (Eq. 4), with e and m anyon transport mediated by external Zeeman fields (h). Junction (a) is transparent to e anyons ($T_e = 1$) and can switch from being opaque ($T_m = 0$) to transparent for m anyons at a threshold field strength h^{th} (purple star in (b)). Junction (c) is opaque to both e and m due to strong quantum fluctuations at the junction from effective pseudospins (see main text).

Excitations in A_v^z are referred to as e charges, while those in B_p^x are called m charges (note that we use a unitarily equivalent definition compared to [46]). We construct a J_1 - J_2 junction (J1J2) (see Fig. 1(a)), where we modify the coupling of B_p^x in a finite intermediate region to J_2 while the rest of the system has coupling J_1 . This renders the junction semi-permeable to tunneling by an m anyon, while it is transparent to an e anyon. A Zeeman field of strength h can selectively induce e or m to tunnel across the junction. While the transmission probability for the e charge $T_e = 1$, the magnetic charge m transmits only beyond a threshold value of $h = h^{\text{th}}$ (see Fig. 1(b)). This should be contrasted with the *phase junction*, where we stitch two otherwise homogeneous TCs, but where in the second region the B_p^x operators are rotated to an arbitrary spin direction $\mathbf{n}_\theta = (\cos \theta, \sin \theta, 0)$, $\theta \in (0, 2\pi)$ (see Fig. 1(c)) such that $B_p^{\mathbf{n}_\theta} = \otimes_{l \in p} \sigma_l \cdot \mathbf{n}_\theta$ (l denotes a link of the lattice). This generically results in a non-

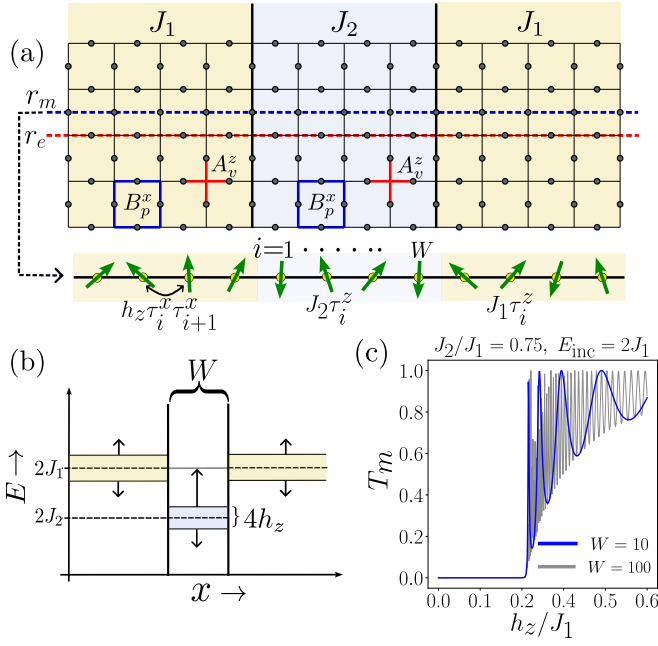


FIG. 2. **The J_1 - J_2 TC junction:** (a) Schematic of lattice model (Eq. (2)) with star (A_v^z) and plaquette (B_p^x) operators. Dynamics of e, m charges induced by Zeeman field along paths r_e and r_m can be mapped to a transverse field Ising chain (Eq. (3)). (b) h_z broadens the m bands leading to a band-mismatch when $J_2 \neq J_1$. (c) Transmission probability (T_m) of m anyons as a function of field (h_z/J_1) shows a jump at a threshold value $h_z = h_z^{\text{th}}$ which is independent of junction size W (data for $E_{\text{inc}} = 2J_1$, $J_2/J_1 = 0.75$, $J_1 = 1$).

commuting junction between the two regions. In this case, even in the absence of any inhomogeneous coupling strengths, the junctions show remarkable opacity to both e and m , which, however, are smoothly tunable by field strength (h) (see Fig. 1(d)). As we will show, both junctions have distinct physical mechanisms leading to their charge-specific permeability.

J1J2 junction: The Hamiltonian is given by

$$H_{J_1 J_2} = -J \sum_v A_v^z - \sum_p J(\mathbf{p}) B_p^x, \quad (2)$$

where $B_p^\alpha = \otimes_{l \in p} \sigma_l^\alpha$ and $A_v^\alpha = \otimes_{l \in v} \sigma_l^\alpha$ are the plaquette p and vertex v operators respectively (and l denotes a link on the lattice), σ^α ($\alpha = x, y, z$) are the Pauli operators. Here, $\mathbf{p} = \{p_x, p_y\}$ denotes the position of a plaquette and $J, J(\mathbf{p}) > 0$. While everywhere else $J(\mathbf{p}) = J_1$, in an intermediate region of width W (indexed $p_x \in \{1, W\}, \forall p_y$) $J(\mathbf{p}) \equiv J_2$ (see Fig. 2(a)). The topologically ordered ground state(s) and the excitations of the standard TC ($J_2 = J_1$) remain stable when $J_2 \neq J_1$. Note that even though all operators mutually commute, crucially, the energy gap for m anyons differs between the J_1 and J_2 regions.

Anyon selective dynamics can be induced by applying an external Zeeman field of strength h_α on specific one-dimensional paths such that $H = H_{J_1 J_2} + H_f^\alpha$ where

$H_f^\alpha = -h_\alpha \sum_l \sigma_l^\alpha$. While a dispersive e charge can be moved by applying an x directional field along row r_e ($\alpha = x$) passing through horizontal links, an m charge can be equivalently moved by action of h_z ($\alpha = z$) on a path r_m cutting the vertical links as shown in Fig. 2(a)). We focus on the limit $h_\alpha/J_1 \ll 1$, ensuring a low-density regime in which anyons are sparsely distributed and associated fluctuations are below the flux gap, allowing us to study their transport at the single-particle level.

The strip of the J_1 - J_2 TC in which the magnetic fields act can be each mapped to a transverse field Ising model (TFIM) [53–55] (see Supplemental Material (SM) [56]). The plaquette and star operators are Ising-like variables, therefore, $A_v^z \mapsto \tau_v^z$, and $B_p^x \mapsto \tau_p^x$. The field causes either anyon hopping or pair creation; hence, $\sim h \tau_i^x \tau_{i+1}^x$ ($i = v/p$). In terms of the τ spins,

$$H^{(q)} = - \sum_{i \in r_q} J_q(i) \tau_i^z - h_\alpha \sum_{i \in r_q} \tau_i^x \tau_{i+1}^x, \quad (3)$$

where $H^{(q)}$ is the effective Hamiltonian describing the dynamics of anyon $q = e, m$. Since h_x (h_z) along r_e (r_m) leads to dynamics only in the e (m) sector, we use the common label α to differentiate them. $J_m(i \in r_m) = J_2$ for $1 \leq i \leq W$ and for the rest of the chain $J_m = J_1$. $J_e(i) = J$ throughout the chain r_e (see lower panel in Fig. 2(a)).

Applying the standard Jordan-Wigner (JW) fermionization followed by a Bogoliubov transformation in the quasi-momentum (k) basis yields the energy dispersion (E_k) of the uniform Ising chain [57]. For $h_\alpha/J_1 \ll 1$ and near the band minimum $k = 0$, $E_k^q \approx \Delta_q + k^2/2M_q$. Here, $\Delta_q = 2|J - h_\alpha|$ is the energy gap and $M_q = |(1 - h_\alpha/J)|/2h_\alpha$ is the band mass of an anyon. At low energies, anyon propagation (with wavefunction ψ_q) is governed by the Schrodinger equation: $-\partial_x^2 \psi_q/2M_q(x) + (V_q(x) - E)\psi_q = 0$ where E is the energy. The e anyon Hamiltonian exhibits translational symmetry: $M_e(x)$ is constant, and the potential $V_e(x) = 0$ throughout the system. Thus, the e anyons freely disperse above the energy gap and $T_e(E) = 1$ for any h_x and incident energy E_{inc} . For the m anyon, $V_m(x) = 2(J_2 - J_1)$ and $M_m(x)$ changes when crossing the J_1 - J_2 boundary; the m anyon is lighter if $J_2 < J_1$ and heavier otherwise. Therefore, the m anyon experiences a junction realizing a *potential barrier/well* with the band mass concomitantly changing across the junction. Moreover, h decides the effective bandwidth of the anyonic bands centered around the bare flux-gap, which is decided by the J_1 or J_2 scale. Thus, tuning h and $J_2 - J_1$ one can mimic the band-pass filter physics of semiconducting systems (see Fig. 2(b)) but now for anyonic transport.

We numerically compute the m -anyon transmission probability $T_m(E, W)$ for arbitrary h_z and E_{inc} using a discretized wavefunction matching (WFM) approach [58] to link eigenstates of the J_1 (leads) and J_2 (scatterer) regions in the JW fermionized Eq. (3) [56]. The main results are summarized in Fig. 2(c). For a fixed $J_2/J_1 = 0.75$ (potential well) and for $E_{\text{inc}} = 2J_1$ (the

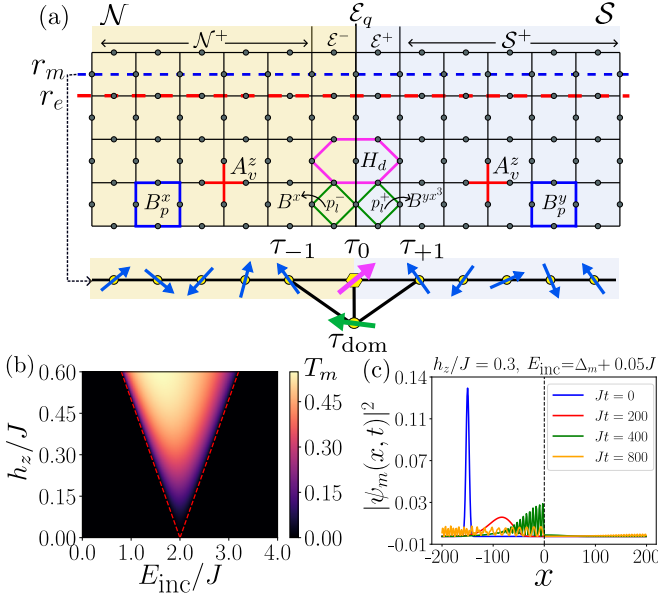


FIG. 3. **The XYJC junction:** (a) The 2D lattice Hamiltonian with its constituent star, plaquette, domino and dimer operators (see Eqs. (4),(7)). Dynamics induced by a Zeeman field along path r_m can be mapped to an Ising chain with a three-spin coupling mediated by an effective pseudospin τ_{dom} . (b) Transmission probability (T_m) for a magnetic charge as a function of field h_z and incident energy E_{inc} . The anyon band edges are shown by red dashed lines. (c) Time evolution snapshots of an m anyon wave packet ($\psi_m(x,t)$) thrown from the \mathcal{N}^+ region towards the junction at different times, showing effective obstruction due to pseudospin ($h_z = 0.3J, E_{\text{inc}} = \Delta_m + 0.05J, J = 1, \Delta_m = 2(J - h_z)$).

zero-field gap of m anyon), we plot T for two different widths ($W = 10$ and $W = 100$) of the J_2 region. Beyond a threshold $h_z^{\text{th}} \approx 0.25J_1$, transmission occurs only through *resonant tunneling*. With increasing W , the number of peaks increases (Fig. 2(c)) as more discrete energy levels (of the J_2 region) match E_{inc} . For $E_{\text{inc}} = 2J_1$, threshold value $h_z^{\text{th}} = J_1 - J_2$ (for $J_2 < J_1$), which is when the upper-band edge of the intermediate region hits the band-bottom of the J_1 regions (also see Fig. 2(b) consistent with this argument). Thus E_{inc} and h_z serve as tuning parameters to modulate anyonic permeability across the junction.

Phase junction: We next consider another class of a TC junction, where two otherwise uniform TCs are stitched to form a non-commuting junction. In the first region (labeled \mathcal{N} for north) we take the usual TC (see Eq. (1)), while in the second region (labeled \mathcal{S} for south) the B_p^x operators are spin-rotated to $B^{n\theta}$ [59]. Note that the set of links (l) on the (vertical) junction line—which we call the equator \mathcal{E}_q —are shared between the two types of B_p operators defined on the two plaquettes, p_l^\pm (see Fig. 3(a)), which do not commute: $[B_{p_l^-}^x, B_{p_l^+}^{n\theta}] \neq 0$ for $\theta \neq 0, l \in \mathcal{E}_q$. When $\theta = \pi/2$, $\{B_{p_l^-}^x, B_{p_l^+}^y\} = 0$ [60], and we refer to this as the *XY junction* (XYJC). This is the

primary focus of this work, with the Hamiltonian,

$$H_{\text{XYJC}} = -J \sum_{p \in \mathcal{N}} B_p^x - J \sum_{p \in \mathcal{S}} B_p^y - J \sum_v A_v^z, \quad (4)$$

forming an anti-commuting junction between the two TCs. It is useful to segregate the microscopic spin operators σ_l^α on the links l into three regions $\{\mathcal{N}, \mathcal{S}, \mathcal{E}_q\}$ depending upon which region they occur. Similarly, the plaquette operators can be conveniently divided into sectors $\{\mathcal{N}^+, \mathcal{S}^+\}$ when all their links exclusively belong to either \mathcal{N} or \mathcal{S} respectively; and $\{\mathcal{E}^-, \mathcal{E}^+\}$ when they share a link with the \mathcal{E}_q line (see Fig. 3(a)). We also rotate H_{XYJC} by

$$U = \prod_{l \in \mathcal{S}} e^{-i\frac{\pi}{4}\sigma_l^z}, \quad (5)$$

which rotates all B_p^y operators in the south to B_p^x , except the ones in the \mathcal{E}^+ region. The transformed Hamiltonian thus becomes

$$\tilde{H}_{\text{XYJC}} = -J \sum_{p \in \mathcal{N}^+, \mathcal{E}^-, \mathcal{S}^+} B_p^x - J \sum_{p \in \mathcal{E}^+} B_p^{yx^3} - \sum_v A_v^z, \quad (6)$$

where $B_p^{yx^3} = UB_p^yU^\dagger = \sigma_{l_\mathcal{E}}^y \otimes_{l \in \mathcal{S}, p} \sigma_l^x$ and $l_\mathcal{E}$ is a link on the equator.

We now introduce two composite Ising-like operators: (1) the *domino*, $D_d = (B_{p_l^-}^x + B_{p_l^+}^{yx^3})/\sqrt{2}$ and (2) the hexagonal-shaped *dimer*, $H_d = B_{p_l^-}^x \otimes B_{p_l^+}^{yx^3}$ where d denotes the rectangular two-plaquette centered on the equatorial link $l_\mathcal{E}$ (see Fig. 3(a)). This allows us to write Eq. (6) as a *frustration-free* Hamiltonian,

$$\tilde{H}_{\text{XYJC}} = -J \sum_{p \in \mathcal{N}^+, \mathcal{S}^+} B_p^x - \sqrt{2}J \sum_{d \in \mathcal{E}_q} D_d - \sum_v A_v^z, \quad (7)$$

Remarkably, the non-commutativity is absorbed in D_d , and the GS is the simultaneous +1 eigenstate of the operators in Eq. (7). In addition to the 4-fold topological degeneracy on a torus (of genus one), there is an additional $O(2^L)$ degeneracy ($L = \text{length of the equator}$), arising from local symmetries ($[H_d, \tilde{H}_{\text{XYJC}}] = 0 \forall d \in \mathcal{E}_q$) (see SM [56]). The degenerate GS manifold is characterized by the ± 1 eigenvalues of H_d . The Hamiltonian, now rewritten as a set of effective stabilizers, is tenable to studying the anyon dynamics, discussed next.

Magnetic (m) charge scattering: As in the J1J2 case, we apply a Zeeman field h_z along a path r_m which passes through the vertical bonds (see Fig. 3(a)). The unitary transformation (Eq. (5)) has no effect on the field. While the z -field coupling (h_z/J) is the same in both the \mathcal{N} and \mathcal{S} regions, operator non-commutativity along the junction leads to a non-trivial tunneling action. To understand the field-induced dynamics, we again go to an Ising model-like description (details in SM [56]). We replace $B_p^x \mapsto \tau_p^z$ ($\forall p \in \mathcal{N}^+, \mathcal{S}^+$), $D_d \mapsto \tau_{\text{dom}}^z$ and $H_d \mapsto \tau_\theta^z$. Away from \mathcal{E}^\pm , σ^z causes either m anyon hopping or pair

creation/annihilation, while in the junction region, it also creates fluctuations in the D_d and H_d sectors, leading to interesting pseudospin (τ_{dom}) dynamics, which in turn, influences anyon transmission.

The τ -spin Hamiltonian is given by,

$$\tilde{H}^{(m)} = H_m + H_{\text{dom}} + H_I^{(1)} + H_I^{(2)}, \quad (8)$$

where

$$H_m = -J \sum_{i \neq 0} \tau_i^z - h_z \sum_{i \notin \{-1, 0\}} \tau_i^x \tau_{i+1}^x, \quad (9)$$

$$H_{\text{dom}} = -\sqrt{2}J \tau_{\text{dom}}^z - h_z \tau_{\text{dom}}^x, \quad (10)$$

$$H_I^{(1)} = -\frac{h_z}{2} [\tau_{-1}^x (\tau_0^x - \tau_0^y) + (\tau_0^x + \tau_0^y) \tau_{+1}^x], \quad (11)$$

$$H_I^{(2)} = -\frac{h_z}{2} [\tau_{-1}^x (\tau_0^x + \tau_0^y) + (\tau_0^x - \tau_0^y) \tau_{+1}^x] \tau_{\text{dom}}^x. \quad (12)$$

This describes a TFIM of τ_i spin- $\frac{1}{2}$ s, coupled to an auxiliary pseudospin τ_{dom} at indices $i = 0, \pm 1$ through three-body terms (see Fig. 3(a), lower panel).

A JW transformation on τ_i , leads to an effective model of a p -wave superconductor coupled to an auxiliary τ_{dom} at the center, amenable to a WFM formalism (see SM [56] for details). This allows us to again numerically calculate the transmission probabilities for the m anyons.

The results are depicted in Fig. 3(b). We find that even at a field of $h_z \sim 0.1J$, at an incident energy $E_{\text{inc}} \sim 2J$ (i.e. at the zero-field flux gap) the transmission probability is small ($T_m \sim 0.1$). This can be monotonically increased by increasing h_z . This high opacity of the junction is surprising given that, unlike in the J1J2 junction, there is no mismatch at the junction in the coupling strengths. To further verify this, we numerically simulate the time evolution of a Gaussian m anyon wave packet ψ_m with the lattice Hamiltonian $\tilde{H}^{(m)}$ (Eq. (8)) for $E_{\text{inc}} \sim \Delta_m$ and $h_z/J \sim 0.3$. As shown in Fig. 3(c), a significant fraction of the wave packet amplitude $|\psi_m|^2$ is reflected back to the $x < 0$ region after hitting the boundary around $Jt \approx 400$.

We next show that this behavior is a direct result of pseudospin (τ_{dom}) fluctuation. A low-energy ($E \sim \Delta_m$) effective theory of m -anyon (ψ) dynamics with Hamiltonian (Eq. (8)) (see derivation in SM [56]) is,

$$\begin{aligned} \tilde{H}^{(m)} \sim & - \int dx \psi^\dagger(x) \left[\Delta(x) + \frac{\partial_x^2}{2M_m} \right] \psi(x) - \mathbf{B}_{\text{eff}} \cdot \boldsymbol{\tau}_{\text{dom}} \\ & + \eta h_z \psi^\dagger(0) \psi(0) \tau_{\text{dom}}^x, \end{aligned} \quad (13)$$

where $\Delta(x) = \Delta_m(1 - \delta(x))$, $\mathbf{B}_{\text{eff}} = \{h_z, 0, \sqrt{2}J\}$, M_m is the band-mass ($\propto h_z^{-1}$) and η is the lattice-regularization coefficient. At $h_z = 0$, as expected, this describes an infinitely heavy particle which is decoupled from a z -polarized τ_{dom} pseudospin. However, as h_z is applied, it induces perturbative x -fluctuations in an otherwise rigid z -polarized τ_{dom} . This leads to a weak transmission of m -anyons whose density at $x = 0$ is determined by both the onsite potential $\Delta(x)$ and fluctuations in τ_{dom} . In

our wave packet simulation we indeed find that a finite, but small transmission of ψ_m is captured in $\langle \tau_{\text{dom}}^x \rangle \neq 0$ (see [56]) thus leading to a significant opacity for the m anyons.

Electric (e) charge scattering: We now discuss the e scattering. As in the J1J2 junction, the Zeeman field ($\propto h_x$) along a path r_e induces e charge dynamics (see Fig. 3(a)). Under the unitary transformation (Eq. (5)) a uniform x -field along r_e is mapped to $h_x \sum_{l \in r_e} [\delta(l \in \mathcal{N}) \sigma_l^x + \delta(l \in \mathcal{S}) \sigma_l^y]$, whose action is to be studied on the Hamiltonian in Eq. (7). A mapping to TFIM, as before, results in two distinct processes in the north and south regions (see SM [56]),

$$H_f^x \mapsto \begin{cases} h_x \sum_i \tau_i^x \tau_{i+1}^x & \forall i \in \{\mathcal{N}^+, \mathcal{E}^-\} \\ h_x \sum_i \tau_i^x (\tau_{i+\frac{1}{2},+}^x \tau_{i+\frac{1}{2},-}^x) \tau_{i+1}^x & \forall i \in \mathcal{S}^+. \end{cases} \quad (14)$$

While the e charges hop freely in the \mathcal{N} region, in the \mathcal{S} region, in addition to hopping, an e charge creates a pair of m charges on the two plaquettes that share the link $(i, i+1)$. These two plaquette operators are described using $\tau_{i+\frac{1}{2}, \pm}$. Furthermore, action of H_f^x on the link $l \in \mathcal{E}^+$ is subtle. Apart from a τ_i^x hopping process, it couples to the pair of domino and dimer operators (see discussion near Eq. (7)) flagging the link [56]. Thus an e charge encounters both pseudo-spin fluctuations near the equator and an m -density dependent hopping in \mathcal{S} region.

In the low-field limit, even though the fluctuations mediated by the degenerate dimer (H_d) excitations allow e charges to traverse the \mathcal{E}^+ region (see [56]); the process governed by Eq. (14) leads to eventual confinement of the e charge. This can be seen by noting that any e charge hopping process in \mathcal{S}^+ over a bond leads to an energy cost of $2\Delta_m \sim 4(J - h_z)$. This leads to a *string tension* for moving the e -anyon on the path r_e inside \mathcal{S}^+ , with the tension growing linearly with the distance traversed. This phenomenon, similar to confinement in gauge theories [56], leads to a rapid fall of T_e with the size of the second region.

Discussion. Our investigation is an initial foray to analyze scattering of Abelian anyons in inhomogeneous \mathbb{Z}_2 spin liquids, for which we consider simple TC variants. As formulated, we have introduced two classes of junctions - one inhomogeneous in the coupling strengths and the other using a set of non-commuting junction operators. These are manifestly semi-permeable and selective, preferentially distinguishing the transport signatures of e and m anyons depending on the initial energy and direction of external field strengths. We have explicitly demonstrated the physical mechanisms behind anyon transmission, which involve effective potential barriers and pseudospin fluctuations. While our work describes \mathbb{Z}_2 charges and one-dimensional scattering paths, a generalization to other Abelian/non-Abelian charges and two-dimensional scattering [61–64] are natural future extensions. Dependence of $T_{e/m}$ on

tuning knob θ in the phase junction is an immediate direction worth pursuing. Although experimental realizations of TCs are few [65–67], the importance of a concrete experimental proposal of TC junctions for tunable anyonic transport cannot be overemphasized.

Acknowledgments: S.B. acknowledges useful discus-

sions with Nicholas O’Dea, Yaodong Li and Jeongwan Haah. S.B. is supported in part by the US Department of Energy, Office of Basic Energy Sciences, Division of Materials Sciences and Engineering, under Contract No. DE-AC02-76SF00515S. S.S. acknowledges support from Institute Postdoctoral Fellowship, IIT Kanpur. Numerical calculations were performed on the workstation *Sherlock* at Stanford University and *Syahi* at IITK.

-
- [1] E Comforti, YC Chung, Moty Heiblum, V Umansky, and Diana Mahalu, “Bunching of fractionally charged quasiparticles tunnelling through high-potential barriers,” *Nature* **416**, 515–518 (2002).
- [2] Cheolhee Han, Jinhong Park, Yuval Gefen, and H-S Sim, “Topological vacuum bubbles by anyon braiding,” *Nature communications* **7**, 11131 (2016).
- [3] James Nakamura, Shuang Liang, Geoffrey C Gardner, and Michael J Manfra, “Direct observation of anyonic braiding statistics,” *Nature Physics* **16**, 931–936 (2020).
- [4] Matteo Carrega, Luca Chirolli, Stefan Heun, and Lucia Sorba, “Anyons in quantum hall interferometry,” *Nature Reviews Physics* **3**, 698–711 (2021).
- [5] Masayuki Hashisaka, Thibaut Jonckheere, Takafumi Akiho, Satoshi Sasaki, Jerome Rech, Thierry Martin, and Koji Muraki, “Andreev reflection of fractional quantum hall quasiparticles,” *Nature communications* **12**, 2794 (2021).
- [6] H. Bartolomei, M. Kumar, R. Bisognin, A. Marguerite, J.-M. Berroir, E. Bocquillon, B. Plaças, A. Cavanna, Q. Dong, U. Gennser, Y. Jin, and G. Fève, “Fractional statistics in anyon collisions,” *Science* **368**, 173–177 (2020).
- [7] Sourav Biswas, Rajarshi Bhattacharyya, Hemanta Kumar Kundu, Ankur Das, Moty Heiblum, Vladimir Umansky, Moshe Goldstein, and Yuval Gefen, “Shot noise does not always provide the quasiparticle charge,” *Nature physics* **18**, 1476–1481 (2022).
- [8] Hemanta Kumar Kundu, Sourav Biswas, Nissim Ofek, Vladimir Umansky, and Moty Heiblum, “Anyonic interference and braiding phase in a mach-zehnder interferometer,” *Nature physics* **19**, 515–521 (2023).
- [9] Bikash Ghosh, Maria Labendik, Vladimir Umansky, Moty Heiblum, and David F. Mross, “Coherent bunching of anyons and their dissociation in interference experiments,” (2024), [arXiv:2412.16316 \[cond-mat.mes-hall\]](https://arxiv.org/abs/2412.16316).
- [10] A Veillon, C Piquard, P Glidic, Y Sato, A Aassime, A Cavanna, Y Jin, U Gennser, A Anthore, and F Pierre, “Observation of the scaling dimension of fractional quantum hall anyons,” *Nature* **632**, 517–521 (2024).
- [11] Zezhu Wei, V. F. Mitrović, and D. E. Feldman, “Thermal interferometry of anyons in spin liquids,” *Phys. Rev. Lett.* **127**, 167204 (2021).
- [12] Kai Klocke, David Aasen, Roger S. K. Mong, Eugene A. Demler, and Jason Alicea, “Time-domain anyon interferometry in kitaev honeycomb spin liquids and beyond,” *Phys. Rev. Lett.* **126**, 177204 (2021).
- [13] Kai Klocke, Joel E. Moore, Jason Alicea, and Gábor B. Halász, “Thermal probes of phonon-coupled kitaev spin liquids: From accurate extraction of quantized edge transport to anyon interferometry,” *Phys. Rev. X* **12**, 011034 (2022).
- [14] Joji Nasu, Yuta Murakami, and Akihisa Koga, “Scattering phenomena for spin transport in a kitaev spin liquid,” *Phys. Rev. B* **106**, 024411 (2022).
- [15] Shi Feng, Adhip Agarwala, Subhro Bhattacharjee, and Nandini Trivedi, “Anyon dynamics in field-driven phases of the anisotropic kitaev model,” *Physical Review B* **108**, 035149 (2023).
- [16] Zezhu Wei, Navketan Batra, V. F. Mitrović, and D. E. Feldman, “Thermal interferometry of anyons,” *Phys. Rev. B* **107**, 104406 (2023).
- [17] Chihiro Harada, Atsushi Ono, and Joji Nasu, “Real-time control of non-abelian anyons in kitaev spin liquid under energy dissipation,” *Phys. Rev. B* **110**, 214426 (2024).
- [18] Gábor B. Halász, “Gate-controlled anyon generation and detection in kitaev spin liquids,” *Phys. Rev. Lett.* **132**, 206501 (2024).
- [19] Shiyu Zhou, Yi Teng, Claudio Chamon, Claudio Castellano, and Armin Rahmani, “Probing anyonic statistics via mach-zehnder interferometry in quantum computers,” (2025), [arXiv:2402.16944 \[quant-ph\]](https://arxiv.org/abs/2402.16944).
- [20] Sebastian Greschner and Luis Santos, “Anyon hubbard model in one-dimensional optical lattices,” *Phys. Rev. Lett.* **115**, 053002 (2015).
- [21] Yuhe Zhang, G. J. Sreejith, and J. K. Jain, “Creating and manipulating non-abelian anyons in cold atom systems using auxiliary bosons,” *Phys. Rev. B* **92**, 075116 (2015).
- [22] Logan W. Clark, Brandon M. Anderson, Lei Feng, Anita Gaj, K. Levin, and Cheng Chin, “Observation of density-dependent gauge fields in a bose-einstein condensate based on micromotion control in a shaken two-dimensional lattice,” *Phys. Rev. Lett.* **121**, 030402 (2018).
- [23] Frederik Görg, Kilian Sandholzer, Joaquín Minguzzi, Rémi Desbuquois, Michael Messer, and Tilman Esslinger, “Realization of density-dependent peierls phases to engineer quantized gauge fields coupled to ultracold matter,” *Nature Physics* **15**, 1161–1167 (2019).
- [24] Vincent Lienhard, Pascal Scholl, Sebastian Weber, Daniel Barredo, Sylvain de Léséleuc, Rukmani Bai, Nicolai Lang, Michael Fleischhauer, Hans Peter Büchler, Thierry Lahaye, and Antoine Browaeys, “Realization of a density-dependent peierls phase in a synthetic, spin-orbit coupled rydberg system,” *Phys. Rev. X* **10**, 021031 (2020).
- [25] Julian Léonard, Sooshin Kim, Joyce Kwan, Perrin Segura, Fabian Grusdt, Cécile Repellin, Nathan Goldman, and Markus Greiner, “Realization of a fractional quantum hall state with ultracold atoms,” *Nature* **619**, 495–499 (2023).

- [26] Joyce Kwan, Perrin Segura, Yanfei Li, Sooshin Kim, Alexey V Gorshkov, André Eckardt, Brice Bakkali-Hassani, and Markus Greiner, “Realization of one-dimensional anyons with arbitrary statistical phase,” *Science* **386**, 1055–1060 (2024).
- [27] Lingnan Shen, Mao Lin, Cedric Yen-Yu Lin, Di Xiao, and Ting Cao, “Realization of fermionic Laughlin state on a quantum processor,” (2025), arXiv:2503.13294 [quant-ph].
- [28] A. J. Willans, J. T. Chalker, and R. Moessner, “Disorder in a quantum spin liquid: Flux binding and local moment formation,” *Phys. Rev. Lett.* **104**, 237203 (2010).
- [29] Fabian Zschöcke and Matthias Vojtá, “Physical states and finite-size effects in Kitaev’s honeycomb model: Bond disorder, spin excitations, and NMR line shape,” *Phys. Rev. B* **92**, 014403 (2015).
- [30] Matthias Vojtá, Andrew K. Mitchell, and Fabian Zschöcke, “Kondo impurities in the Kitaev spin liquid: Numerical renormalization group solution and gauge-flux-driven screening,” *Phys. Rev. Lett.* **117**, 037202 (2016).
- [31] Joji Nasu and Yukitoshi Motome, “Thermodynamic and transport properties in disordered Kitaev models,” *Phys. Rev. B* **102**, 054437 (2020).
- [32] Wen-Han Kao, Johannes Knolle, Gábor B. Halász, Roderich Moessner, and Natalia B. Perkins, “Vacancy-induced low-energy density of states in the Kitaev spin liquid,” *Phys. Rev. X* **11**, 011034 (2021).
- [33] Vitor Dantas and Eric C. Andrade, “Disorder, low-energy excitations, and topology in the Kitaev spin liquid,” *Phys. Rev. Lett.* **129**, 037204 (2022).
- [34] Suheon Lee, YS Choi, S-H Do, Wonjun Lee, CH Lee, Minseong Lee, M Vojtá, CN Wang, H Luetkens, Z Guguchia, *et al.*, “Kondo screening in a Majorana metal,” *Nature Communications* **14**, 7405 (2023).
- [35] Alexei Kitaev and Liang Kong, “Models for gapped boundaries and domain walls,” *Communications in Mathematical Physics* **313**, 351–373 (2012).
- [36] Héctor Bombín, “Topological order with a twist: Ising anyons from an abelian model,” *Physical Review Letters* **105**, 030403 (2010).
- [37] Maïssam Barkeshli, Chao-Ming Jian, and Xiao-Liang Qi, “Theory of defects in abelian topological states,” *Phys. Rev. B* **88**, 235103 (2013).
- [38] Jeffrey C. Y. Teo, Abhishek Roy, and Xiao Chen, “Unconventional fusion and braiding of topological defects in a lattice model,” *Phys. Rev. B* **90**, 115118 (2014).
- [39] Tian Lan, Juven C Wang, and Xiao-Gang Wen, “Gapped domain walls, gapped boundaries, and topological degeneracy,” *Physical Review Letters* **114**, 076402 (2015).
- [40] Olga Petrova, Paula Mellado, and Oleg Tchernyshyov, “Unpaired Majorana modes on dislocations and string defects in Kitaev’s honeycomb model,” *Phys. Rev. B* **90**, 134404 (2014).
- [41] Jacob C Bridgeman, Stephen D Bartlett, and Andrew C Doherty, “Tensor networks with a twist: Anyon-permuting domain walls and defects in projected entangled pair states,” *Physical Review B* **96**, 245122 (2017).
- [42] Maïssam Barkeshli, Erez Berg, and Steven Kivelson, “Coherent transmutation of electrons into fractionalized anyons,” *Science* **346**, 722–725 (2014).
- [43] Elio J. König, Mallika T. Randeria, and Berthold Jäck, “Tunneling spectroscopy of quantum spin liquids,” *Phys. Rev. Lett.* **125**, 267206 (2020).
- [44] Gilad Kishony and Erez Berg, “Converting electrons into emergent fermions at a superconductor–Kitaev spin liquid interface,” *Phys. Rev. B* **104**, 235118 (2021).
- [45] Gautam Nambiar, Daniel Bulmash, and Victor Galitski, “Monopole Josephson effects in a Dirac spin liquid,” *Phys. Rev. Res.* **5**, 013169 (2023).
- [46] A Yu Kitaev, “Fault-tolerant quantum computation by anyons,” *Annals of Physics* **303**, 2–30 (2003).
- [47] Lucile Savary and Leon Balents, “Quantum spin liquids: a review,” *Reports on Progress in Physics* **80**, 016502 (2016).
- [48] Xiao-Gang Wen, “Colloquium: Zoo of quantum-topological phases of matter,” *Rev. Mod. Phys.* **89**, 041004 (2017).
- [49] JM Leinaas and J Myrheim, “On the theory of identical particles,” *Il nuovo cimento* **37**, 132 (1977).
- [50] Frank Wilczek, *Fractional statistics and anyon superconductivity*, Vol. 5 (World Scientific, 1990).
- [51] F. D. M. Haldane, ““fractional statistics” in arbitrary dimensions: A generalization of the Pauli principle,” *Phys. Rev. Lett.* **67**, 937–940 (1991).
- [52] Chetan Nayak, Steven H. Simon, Ady Stern, Michael Freedman, and Sankar Das Sarma, “Non-abelian anyons and topological quantum computation,” *Rev. Mod. Phys.* **80**, 1083–1159 (2008).
- [53] Simon Trebst, Philipp Werner, Matthias Troyer, Kirill Shtengel, and Chetan Nayak, “Breakdown of a topological phase: Quantum phase transition in a loop gas model with tension,” *Phys. Rev. Lett.* **98**, 070602 (2007).
- [54] Dimitris I. Tsomokos, Tobias J. Osborne, and Claudio Castelnovo, “Interplay of topological order and spin glassiness in the toric code under random magnetic fields,” *Phys. Rev. B* **83**, 075124 (2011).
- [55] Mohammad Hossein Zarei, “Ising order parameter and topological phase transitions: Toric code in a uniform magnetic field,” *Phys. Rev. B* **100**, 125159 (2019).
- [56] See Supplementary Material at [url] for details on the analytical and numerical calculations discussed in the main text.
- [57] Subir Sachdev, *Quantum Phase Transitions*, 2nd ed. (Cambridge University Press, 2011).
- [58] PA Khomyakov, G Brocks, Volodymyr Karpan, M Zwierzycki, and Paul J Kelly, “Conductance calculations for quantum wires and interfaces: Mode matching and Green’s functions,” *Physical Review B—Condensed Matter and Materials Physics* **72**, 035450 (2005).
- [59] The \mathcal{N}, \mathcal{S} nomenclature for the two regions is inspired by considering the toric code on a manifold of genus 0 (a sphere such as the Earth). The junction line is thus called the equator \mathcal{E}_q .
- [60] A study of the model for general θ , including an opacity of the barriers as a function of θ will be reported elsewhere. We mention here that for arbitrary θ , $[B_{p_i^-}^x, B_{p_i^+}^{\theta}] = 2i \sin \theta \sigma_i^z H_d$ (see above Eq. 6 for the definition of the H_d operator).
- [61] Oliver Hart, Yuan Wan, and Claudio Castelnovo, “Correlation holes and slow dynamics induced by fractional statistics in gapped quantum spin liquids,” *Nature Communications* **12**, 1459 (2021).
- [62] Matthew Stern, Claudio Castelnovo, Roderich Moessner, Vadim Oganesyan, and Sarang Gopalakrishnan, “Quantum percolation of monopole paths and the response of quantum spin ice,” *Phys. Rev. B* **104**, 115114 (2021).

- [63] Max McGinley, Michele Fava, and S. A. Parameswaran, “Anomalous thermal relaxation and pump-probe spectroscopy of two-dimensional topologically ordered systems,” *Phys. Rev. B* **109**, 075108 (2024).
- [64] Xu Yang, Ryan Buechele, and Nandini Trivedi, “Detection of anyon braiding through pump-probe spectroscopy,” (2025), arXiv:2503.22792 [cond-mat.str-el].
- [65] G. Semeghini et al, “Probing topological spin liquids on a programmable quantum simulator,” *Science* **374**, 1242–1247 (2021).
- [66] KJ Satzinger, Y-J Liu, A Smith, C Knapp, M Newman, C Jones, Zhaoshi Chen, Céline Quintana, Xiaohua Mi, A Dunsworth, *et al.*, “Realizing topologically ordered states on a quantum processor,” *Science* **374**, 1237–1241 (2021).
- [67] Mohsin Iqbal, Nathanan Tantivasadakarn, Ruben Verresen, Sara L Campbell, Joan M Dreiling, Caroline Figgatt, John P Gaebler, Jacob Johansen, Michael Mills, Steven A Moses, *et al.*, “Non-abelian topological order and anyons on a trapped-ion processor,” *Nature* **626**, 505–511 (2024).
- [68] A Yu Kitaev, “Unpaired majorana fermions in quantumwires,” *Physics-uspekhi* **44**, 131 (2001).

Supplemental Material for: Tunable anyonic permeability across \mathbb{Z}_2 spin liquid junctions

Contents

References	5
I. Mapping of the J_1 - J_2 junction in a Zeeman field to an Ising chain	8
II. Properties of XY junction: zero-field ground states and topological degeneracy	9
III. Derivation of effective spin-chain models governing field-induced anyon dynamics in the XY junction	10
A. Field-induced dynamics of m anyons	11
B. Field-induced dynamics of e anyons	13
IV. Jordan-Wigner fermionization of the spin chain model describing m anyon dynamics in XY toric code junction	14
V. Wavefunction matching formalism for calculating transmission probability	15
VI. Continuum description of $\tilde{H}^{(m)}$	18
VII. Mapping e anyon dynamics to a 1d \mathbb{Z}_2 gauge theory	19

I. Mapping of the J_1 - J_2 junction in a Zeeman field to an Ising chain

As outlined in the main text (see Sec. J1J2 junction), the plaquette (B_p^x) and star (A_v^z) operators are Ising-like variables [53–55], located at the plaquette centers and vertices of the square lattice, respectively. Therefore, $B_p^x \mapsto \tau_p^z$ and $A_v^z \mapsto \tau_v^z$, where $\tau_{p/v}^z$ are Pauli operators with eigenvalues ± 1 . We next derive the effective actions of the Zeeman terms $-h_\alpha \sum_l \sigma_l^\alpha$ in terms of the τ spins. In general, the “gauge spins” (σ_l^α) cannot be fully eliminated due to the long-range statistical interaction between e and m anyons [47]. However, in our setup, the magnetic field acts along distinct one-dimensional chains. Consequently, the mutual statistics between e and m anyons do not influence their behavior, allowing them to act as ordinary bosonic particles.

The field along the x -direction only causes fluctuations in the e sector. To derive its action, we determine what σ^x does to a general eigenstate of the zero-field toric code, when m charges are totally absent. A general eigenstate in the zero m sector is given by,

$$|r_1^v, r_2^v, \dots, r_N^v\rangle = \prod_{i \in v} (1 + (-1)^{r_i^v} A_i^z) |\uparrow\uparrow\uparrow \dots \uparrow\rangle_x, \quad (\text{S1})$$

where $r_i^v = 0$ or 1 for $i \in [1, N]$. The action of A_j^z and σ_l^x ($l \equiv \langle j, j+1 \rangle$) are

$$A_j^z |r_1^v, r_2^v, \dots, r_N^v\rangle = (-1)^{r_j^v} |r_1^v, r_2^v, \dots, r_N^v\rangle, \quad (\text{S2})$$

$$\sigma_l^x |r_1^v, r_2^v, \dots, r_N^v\rangle = |r_1^v, \dots, r_j^v + 1, r_{j+1}^v + 1, \dots, r_N^v\rangle, \quad (\text{S3})$$

where addition is defined modulo 2. Therefore,

$$\sigma_l^x \equiv \sigma_{j,j+1}^x \mapsto \tau_j^x \tau_{j+1}^x, \quad (\text{S4})$$

where τ_j^x represents the e anyon creation operator at vertex j . While our study is in the zero-flux sector, the mapping is valid even in the presence of any (static) background m charges. Here, given that the field is along a specific path, a unitary transformation on a set of σ s can make the spins along that path x polarized.

Similarly, to get the field-induced dynamics for the m anyons, we consider the state $|r_1^p, r_2^p, \dots, r_N^p\rangle = \prod_{i \in v} (1 + (-1)^{r_i^p} B_i^x) |\uparrow\uparrow\uparrow \dots \uparrow\rangle_z$ and see how it changes under σ_l^z . We again find $B_p^x \mapsto \tau_p^z$ and $\sigma_l^z \mapsto \tau_p^x \tau_{p+1}^x$, where the dual

lattice link $(p, p+1)$ is perpendicular to the (direct lattice) link, l .

Note that the above mapping retains the algebra of the original operators. For instance, $\{B_p^x, \sigma_e^z\} = 0$ if they share a common link and commute otherwise; this is true for the τ spins as well since $[\tau_{p(v)}^z, \tau_{p'(v')}^x \tau_{p''(v'')}^x] = 0$ if $p(v) \neq p'(v'), p''(v'')$ and anti-commute otherwise.

II. Properties of XY junction: zero-field ground states and topological degeneracy

The Hamiltonian of the XY junction (XYJC) model, in the absence of any external magnetic fields, is defined as follows

$$H_{\text{XYJC}} = -J \sum_{p \in \mathcal{N}} B_p^x - J \sum_{p \in \mathcal{S}} B_p^y - J \sum_v A_v^z, \quad (\text{S5})$$

In the \mathcal{N} region, we have the usual toric code, but the spin basis is rotated (with respect to the z -axis) by $\pi/2$ in the \mathcal{S} region (see the notations in Fig. (3) of the main text). Hence, $B_p^y = \prod_{l \in p} \sigma_l^y$, for $p \in \mathcal{S}$. We rotate all spin operators on the right of the equator line (\mathcal{E}_q) by $U = \prod_{l \in \mathcal{S}} e^{-i\frac{\pi}{4}\sigma_l^z}$. Therefore, the Hamiltonian transforms to

$$U^\dagger H_{\text{XYJC}} U = \tilde{H}_{\text{XYJC}} = -J \sum_{p \in \mathcal{N}^+, \mathcal{E}^-, \mathcal{S}^+} B_p^x - J \sum_{p \in \mathcal{E}^+} B_p^{yx^3} - \sum_v A_v^z, \quad (\text{S6})$$

where $B_p^{yx^3} = U B_p^y U^\dagger = \sigma_{l_\mathcal{E}}^y \otimes_{l \in \mathcal{S}, p} \sigma_l^x$, $l_\mathcal{E}$ is a link on the equator (\mathcal{E}_q) and \mathcal{N}^+ (\mathcal{S}^+) is the set of north (south) plaquettes excluding p_l^- (p_l^+); these plaquettes are inside \mathcal{E}^\pm (Fig. (3), main text). A more convenient description of this Hamiltonian is obtained by the introduction of the *domino* operators,

$$\tilde{H}_{\text{XYJC}} = -J \sum_{p \in \mathcal{N}^+, \mathcal{S}^+} B_p^x - \sqrt{2}J \sum_{d \in \mathcal{E}_q} D_d - \sum_v A_v^z, \quad (\text{S7})$$

where $D_d = (B_{p_l^-}^x + B_{p_l^+}^{yx^3})/\sqrt{2}$ is called the *domino* operator and satisfies the following algebraic relations: (1) $D_d^2 = 1$, (2) $[D_{d_1}, D_{d_2}] = 0$ for any two domino plaquettes $d_1, d_2 \in \mathcal{E}_q$, and (3) $[D_d, B_p^x] = [D_d, A_v^z] = 0$. Thus, all the *stabilizer* operators commute and the exact ground state is obtained by minimizing the individual terms of the Hamiltonian (Eq.(S7)).

The *dimer* operator $H_d = B_{p_l^-}^x \otimes B_{p_l^+}^x$ is a symmetry of Eq. (S7). A single *dimer* excitation, obtained by flipping one H_d eigenvalue ($= (-1)^{r_d^h}$, where $r_d^h = 0/1$), does not cost any energy. This enables the ground state to host an arbitrary number of these quasiparticles. This leads to a substantial ground state degeneracy ($\sim 2^{L_y}$), with the degenerate manifold defined by the set $\{r_d^h\}$, $\forall d \in \mathcal{E}_q$. The explicit forms of these states are

$$|\text{GS}, \{r_d^h\}_{d \in \mathcal{E}_q}\rangle = \prod_{d \in \mathcal{E}_q} (1 + (-1)^{r_d^h} H_d) (1 + D_d) \prod_{p \in \mathcal{N}^+, \mathcal{S}^+} (1 + B_p^x) \bigotimes_l |\uparrow\rangle_l^z \quad (\text{S8})$$

If the model is defined on a torus (i.e., there are two junctions between the *rotated* and *unrotated* regions), there is an additional restriction on the set $\{r_d^h\}$. This is due to the condition,

$$\prod_{d \in \mathcal{E}_q} H_d = \prod_{p \in \mathcal{N}^+, \mathcal{S}^+} B_p^x \quad (\text{S9})$$

which tells us that the net parity of dimer excitations along the equator is fixed by the total m charge parity in the rest of the system. The GS must not have m charges inside $\{\mathcal{N}^+, \mathcal{S}^+\}$, which implies $\prod_{d \in \mathcal{E}_q} H_d |\text{GS}\rangle = (+1) |\text{GS}\rangle$ [Nevertheless, the XYJC ground state contains a finite density of m anyons within $\mathcal{E}^- \cup \mathcal{E}^+$, due to operator non-commutativity. Through a straightforward analytical calculation, we determine that the average density of m anyons, $n_m^\mathcal{E}$ ranges from $n_m^{\min} = \sin^2(\pi/8)$ to $n_m^{\max} = \sin^2(\pi/4)$]. Hence, the physical ground states (on a torus) are given by

$$\left| \text{GS}, \{r_d^h\}_{d \in \mathcal{E}_q}, (-1)^{\sum_d r_d^h} = 1 \right\rangle = (1 + \prod_{d \in \mathcal{E}_q} H_d) |\text{GS}, \{r_d^h\}_{d \in \mathcal{E}_q}\rangle \quad (\text{S10})$$

The GS degeneracy is therefore 2^{2L_y-1} , where $2L_y$ = the total length of the equator (\mathcal{E}_q) for the lattice with periodic boundary conditions.

Topological degeneracy:

The ground state (GS) degeneracy discussed so far arises from the local symmetries (H_d) inherent to our junction model and is unrelated to the topology of the spatial manifold on which the model is defined. As we will elaborate, the topological degeneracy of the phase-junction ground state remains identical to that of the standard toric code. Consequently, the four distinct topological sectors of excitations ($1, e, m, \psi$) observed in the canonical toric code are preserved.

Define two toric cycle operators (*Wilson loops*) that act non-trivially on the XYJC ground state, Eq. (S10), given by

$$W_x = \prod_{l \in C_x} (\sigma_l^x)^{1-\delta_{l, \text{leq}}} \left(\frac{\sigma_l^x + \sigma_l^y}{\sqrt{2}} \right)^{\delta_{l, \text{leq}}} \quad \text{and} \quad W_y = \prod_{l \in C_y} (\sigma_l^x)^{1-\delta_{l, \text{leq}}} \left(\frac{\sigma_l^x + \sigma_l^y}{\sqrt{2}} \right)^{\delta_{l, \text{leq}}}. \quad (\text{S11})$$

Here, $C_{x,y}$ denote two non-contractible closed loops of the torus that pass through the bonds of the square lattice. For every link, $l \in C_{x,y}$, we apply σ_l^x . However, when parts of the loops lie along the equator (i.e., if $l = l_{\mathcal{E}}$ for $l_{\mathcal{E}} \in \mathcal{E}_q$), σ_l^x is replaced by the operator inside the brackets of Eq. (S11). Here, δ_{l_1, l_2} denotes the Kronecker delta. The fourfold degenerate ground states are given by the states,

$$|\mu, \nu\rangle = (W_x)^\mu (W_y)^\nu \left| \text{GS}, \{r_d^h\}_{d \in \mathcal{E}_q}, (-1)^{\sum_d r_d^h} = 1 \right\rangle, \quad (\text{S12})$$

where μ, ν take the values 0 and 1. The other set of loop operators (*'t Hooft loops*) that equivalently characterize the above four degenerate states are those of the canonical toric code,

$$V_x = \prod_{l \in \tilde{C}_x} \sigma_l^z, \quad V_y = \prod_{l \in \tilde{C}_y} \sigma_l^z, \quad (\text{S13})$$

where $\tilde{C}_{x,y}$ are the contours that pass through the dual square lattice, intersecting the direct lattice links. One can easily verify that $|0, 0\rangle \equiv |v_x = +1, v_y = +1\rangle$, $|0, 1\rangle \equiv |v_x = -1, v_y = +1\rangle$, $|1, 0\rangle \equiv |v_x = +1, v_y = -1\rangle$, and $|1, 1\rangle \equiv |v_x = -1, v_y = -1\rangle$, where v_x and v_y are the eigenvalues of V_x and V_y respectively.

III. Derivation of effective spin-chain models governing field-induced anyon dynamics in the XY junction

The Hamiltonian for the XY junction subjected to external magnetic fields is given as follows,

$$H = H_{\text{XYJC}} - h_z \sum_{l \in r_m} \sigma_l^z - h_x \sum_{l \in r_e} \sigma_l^x. \quad (\text{S14})$$

Here, r_m and r_e are different one dimensional contours, respectively, along which the σ^z and σ^x operators act (see Fig. (3) of the main text). Since anyonic motion is restricted to one dimensional chains, we separate the two dimensional Hamiltonian (H) into two parts, $H = H'_0[p \notin r_m, v \notin r_e] + H_{\text{ladder}}$, where

$$H_{\text{ladder}} = -J \sum_{p \in r_m} \left[B_p^x \delta(p \in \mathcal{N}) + B_p^y \delta(p \in \mathcal{S}) \right] - J \sum_{v \in r_e} A_v^z - h_z \sum_{l \in r_m} \sigma_l^z - h_x \sum_{l \in r_e} \sigma_l^x \quad (\text{S15})$$

Here, the sum over p corresponds to the plaquettes cut by the r_m string, and similarly, the sum over v corresponds to vertices positioned on the r_e string. As in the zero-field case, we rotate the spins (from y to x) in the \mathcal{S} region,

$$U^\dagger H_{\text{ladder}} U = \tilde{H}_{\text{ladder}} = \tilde{H}^{(m)} + \tilde{H}^{(e)} \quad (\text{S16})$$

where

$$\tilde{H}^{(m)} = -J \sum_{p \in r_m} \left[\sum_{p \in \mathcal{N}^+, \mathcal{S}^+} B_p^x + \sqrt{2} \sum_{p \in \mathcal{E}_q} D_d \right] - h_z \sum_{l \in r_m} \sigma_l^z \quad (\text{S17})$$

$$\tilde{H}^{(e)} = -J \sum_{v \in r_e} A_v^z - h_x \sum_{l \in r_e} [\delta(l \in \mathcal{N}) \sigma_l^x - \delta(l \in \mathcal{S}) \sigma_l^y] \quad (\text{S18})$$

In this section, we derive the effective 1D Hamiltonians in terms of τ spins that describe the dynamics of m and e anyons across the junction. The method is similar to what we have already done for the J_1 - J_2 model (Sec. I). The z - and x -directional magnetic fields are confined to distinct one-dimensional strings, eliminating the need to account for the long-range interaction between e and m anyons arising from their semionic statistics during the derivation of the effective Hamiltonian.

A. Field-induced dynamics of m anyons

We first consider the action of $-h_z \sum_{l \in r_m} \sigma_l^z$ on the zero-field XYJC. Since σ_l^z does not cause any fluctuations in the e sector, we consider an arbitrary eigenstate of the XYJC in the e charge-free sector ($A_v^z = +1 \forall v$) and find out how σ_l^z modifies it. These eigenstates are labeled by the eigenvalues of B_p^x , D_d and H_d ,

$$\begin{aligned} |\{r_d^h\}'_{d \in \mathcal{E}_q}, \{r_d\}_{d \in \mathcal{E}_q}, \{r_p\}_{p \in (\mathcal{N}^+, \mathcal{S}^+)}\rangle &= \left(1 + (-1)^{\sum_{p \in (\mathcal{N}^+, \mathcal{S}^+)} r_p} \prod_{d \in \mathcal{E}_q} H_d \right) \\ &\times \prod_{d \in \mathcal{E}_q} (1 + (-1)^{r_d^h} H_d) (1 + (-1)^{r_d} D_d) \prod_{p \in (\mathcal{N}^+, \mathcal{S}^+)} (1 + (-1)^{r_p} B_p^x) \bigotimes_l |\uparrow\rangle_l^z, \end{aligned} \quad (\text{S19})$$

This state gives the eigenvalues $H_d = (-1)^{r_d^h}$, $D_d = (-1)^{r_d}$, and $B_p^x = (-1)^{r_p}$ in their respective domains of action. The first projection operator ensures that we remain in the physical subspace because the H_d projection could give rise to state components that change the m charge parity (or the eigenvalue of $\prod_{p \in \mathcal{N}^+, \mathcal{S}^+} B_p^x$) and therefore such states must be killed. With open boundary conditions, there are no constraints on $\{r_d^h\}$, and we take this boundary condition for the subsequent calculations.

First, we replace all the Ising-like plaquette operators by Pauli- z operators: (1) $B_p^x \mapsto \tau_p^z$ (for $p \in \mathcal{N}^+, \mathcal{S}^+$), (2) $D_d \mapsto \tau_{\text{dom}}^z$, and (3) $H_d \mapsto \mathcal{H}_d^z$ (for $d \in \mathcal{E}_q$).

(A) *Action of σ_l^z in the bulk of \mathcal{N}^+ , \mathcal{S}^+ regions:* In this case, σ_l^z creates m anyons on the two plaquettes that share the common link l . Mathematically, this is expressed as

$$\sigma_l^z |\{r_d^h\}_{d \in \mathcal{E}_q}, \{r_d\}_{d \in \mathcal{E}_q}, \{r_p\}'_{d \in (\mathcal{N}^+, \mathcal{S}^+)}\rangle = |\{r_d^h\}_{d \in \mathcal{E}_q}, \{r_d\}_{d \in \mathcal{E}_q}, \{r_p\}'_{d \in (\mathcal{N}^+, \mathcal{S}^+)}, r_p + 1, r_{p'} + 1\rangle, \quad (\text{S20})$$

where the bond $\langle pp' \rangle$ is perpendicular to the edge l . The prime symbol above $\{r_p\}$ implies that the set excludes the plaquettes p and p' . Therefore, in terms of the τ spins, the action of σ_l^z is given by,

$$\sigma_l^z \mapsto \tau_p^x \tau_{p'}^x. \quad (\text{S21})$$

(B) *Action of σ_l^z on the boundary between $\mathcal{E} = \mathcal{E}^- \cup \mathcal{E}^+$ and $(\mathcal{N}^+, \mathcal{S}^+)$ regions:* Here, the action of σ_l^z is non-trivial; besides creating one m charge, it also flips one of the H_d eigenvalues and converts the D_d operator to a new operator $D'_d = (B_{p_l^-}^x - B_{p_l^+}^{x^3 y})/\sqrt{2}$, which commutes with all other operators except D_d . In fact, with D_d it anti-commutes— $\{D_d, D'_d\} = 0$.

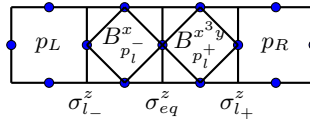


FIG. S1. A small slice of the XYJC model, showing the action of $\sigma_{l_{\pm}}^z$ and σ_{eq}^z in the \mathcal{E} region.

For the link l_- that resides at the left boundary of the domino (\mathcal{E}) region, the explicit expression for the action of

$\sigma_{l_-}^z$ on the general energy eigenstate (Eq. (S19)) of the zero e charge sector is given by,

$$\begin{aligned} \sigma_{l_-}^z |\{r_d^h\}_{d \in \mathcal{E}_q}, \{r_d\}_{d \in \mathcal{E}_q}, \{r_p\}_{p \in (\mathcal{N}^+, \mathcal{S}^+)}\rangle &= \left[1 + (-1)^{r_d^h + 1} H_d \right] \prod'_{d' \in \mathcal{E}_q} \left[1 + (-1)^{r_{d'}^h} H_{d'} \right] \\ &\times \left[1 + \frac{(-1)^{r_d + 1}}{\sqrt{2}} D'_d \right] \prod'_{d' \in \mathcal{E}_q} \left[1 + \frac{(-1)^{r_{d'}}}{\sqrt{2}} D_{d'} \right] \left[1 + (-1)^{r_{p_L} + 1} B_{p_L}^x \right] \prod'_{p' \in \mathcal{N}^+, \mathcal{S}^+} \left[1 + (-1)^{r_{p'}} B_{p'}^x \right] \bigotimes_l |\uparrow\rangle_l^z. \end{aligned} \quad (\text{S22})$$

Therefore, $\sigma_{l_-}^z$ flips the $B_{p_L}^x$ plaquette placed on the left of the link l_- . It also flips the eigenvalues of H_d and D_d , but simultaneously changes the operator $\sqrt{2}D_d (= B_{p_i}^x + B_{p_i^+}^{x^3y})$ to $\sqrt{2}D'_d (= B_{p_i}^x - B_{p_i^+}^{x^3y})$. The prime symbol above the products indicates that the flipped domino index d and the plaquette p_L are excluded.

Since $\sigma_{l_-}^z$ acts locally (i.e., it only changes the eigenvalues of the nearby plaquette operators), we use a simplified labeling of these eigenstates. We label $|\{r_d^h\}_{d \in \mathcal{E}_q}, \{r_d\}_{d \in \mathcal{E}_q}, \{r_p\}_{p \in (\mathcal{N}^+, \mathcal{S}^+)}\rangle \equiv |r_d^h, r_{p_L}, r_d\rangle$. Therefore, the general eigenstate (in the $A_v^z = 1$ sector) is labeled by the eigenvalues of H_d , D_d , and $B_{p_L}^x$ operators that share a common link with $\sigma_{l_-}^z$. It is obvious that the state $\sigma_{l_-}^z |r_{p_L}, r_d^h, r_d\rangle$ can have non-zero overlaps *only* with the states having $r_d^h + 1$ and $r_{p_L} + 1 \pmod{2}$. Hence, the effective actions in these two cases are just *spin-flip* operations described by \mathcal{H}_d^x and $\tau_{p_L}^x$. To figure out what happens in the domino ($\{r_d\}$) subspace, we have to evaluate the following two overlaps (A) and (B),

$$(A) \quad \langle r_d^h + 1, r_{p_L} + 1, r_d | \sigma_{l_-}^z | r_d^h, r_{p_L}, r_d \rangle, \quad (\text{S23})$$

$$(B) \quad \langle r_d^h + 1, r_{p_L} + 1, r_d + 1 | \sigma_{l_-}^z | r_d^h, r_{p_L}, r_d \rangle, \quad (\text{S24})$$

that measure the extent of flipping of the domino operator. A straightforward calculation yields,

$$\langle r_d^h + 1, r_{p_L} + 1, r_d | \sigma_{l_-}^z | r_d^h, r_{p_L}, r_d \rangle = \frac{1}{\sqrt{2}} \exp \left[-i \frac{\pi}{4} (-1)^{r_d^h} \right], \quad (\text{S25})$$

$$\langle r_d^h + 1, r_{p_L} + 1, r_d + 1 | \sigma_{l_-}^z | r_d^h, r_{p_L}, r_d \rangle = \frac{1}{\sqrt{2}} \exp \left[i \frac{\pi}{4} (-1)^{r_d^h} \right]. \quad (\text{S26})$$

Therefore, the effective action of $\sigma_{l_-}^z$ is the following,

$$\sigma_{l_-}^z \mapsto \frac{1}{\sqrt{2}} \tau_{p_L}^x \mathcal{H}_d^x (e^{i \frac{\pi}{4} \mathcal{H}_d^z} \tau_{\text{dom}}^x + e^{-i \frac{\pi}{4} \mathcal{H}_d^z} \mathbb{1}) = \frac{1}{2} (1 + \tau_{\text{dom}}^x) \tau_{p_L}^x \mathcal{H}_d^x - \frac{1}{2} (1 - \tau_{\text{dom}}^x) \tau_{p_L}^x \mathcal{H}_d^y. \quad (\text{S27})$$

The steps of obtaining the action of $\sigma_{l_+}^z$ are almost the same as those done for $\sigma_{l_-}^z$, except for a change in the signs of the phase factors, because,

$$\sigma_{l_+}^z \left(1 + (-1)^{r_d} \frac{D}{\sqrt{2}} \right) = \left(1 + (-1)^{r_d} \frac{D'}{\sqrt{2}} \right) \sigma_{l_+}^z. \quad (\text{S28})$$

This is in contrast to the case where $\sigma_{l_-}^z$ is passed through D_d ; there, the operator $\sqrt{2}D_d (= B_{p_i}^x + B_{p_i^+}^{x^3y})$ converts to $\sqrt{2}D'_d (= B_{p_i}^x - B_{p_i^+}^{x^3y})$ with an extra minus sign. This extra phase also enters in the overlaps, and as a consequence,

$$\sigma_{l_+}^z \mapsto \frac{1}{\sqrt{2}} \tau_{p_R}^x \mathcal{H}_d^x (e^{-i \frac{\pi}{4} \mathcal{H}_d^z} \tau_{\text{dom}}^x + e^{i \frac{\pi}{4} \mathcal{H}_d^z} \mathbb{1}) = \frac{1}{2} (1 + \tau_{\text{dom}}^x) \mathcal{H}_d^x \tau_{p_R}^x + \frac{1}{2} (1 - \tau_{\text{dom}}^x) \mathcal{H}_d^y \tau_{p_R}^x. \quad (\text{S29})$$

(C) *Action of the $\sigma_{l_-}^z$ operator that lives on the equator:* We call this spin σ_{eq}^z . In this case, $\{\sigma_{\text{eq}}^z, D_d\} = 0$, but commute with the rest of the operators present in the Hamiltonian and with H_d . Therefore,

$$\sigma_{\text{eq}}^z \mapsto \tau_{\text{dom}}^z \quad (\text{S30})$$

We now express the Hamiltonian (Eq.(S17)) that describes the m charge dynamics, in terms of the dual ($\tau_p^\alpha, \tau_{\text{dom}}^\alpha$ and \mathcal{H}_d^α) spins. Using Eqs. (S21), (S27), (S29), and (S30), we obtain the following,

$$\begin{aligned} \tilde{H}^{(m)} &= -J \sum_{p \in \mathcal{N}^+, \mathcal{S}^+} \tau_p^z - h_z \sum_{\substack{p \in \mathcal{N}^+, \mathcal{S}^+ \\ p \neq p_L, p_1^+}} \tau_p^x \tau_{p+1}^x - (\sqrt{2}J \tau_{\text{dom}}^z + h_z \tau_{\text{dom}}^x) \\ &- \frac{h_z}{2} \left\{ (\tau_{p_L}^x + \tau_{p_R}^x) \mathcal{H}_d^x (\tau_{\text{dom}}^x + \mathbb{1}) + (\tau_{p_L}^x - \tau_{p_R}^x) \mathcal{H}_d^y (\tau_{\text{dom}}^x - \mathbb{1}) \right\} \end{aligned} \quad (\text{S31})$$

The first sum (over plaquettes (p)) excludes p_l^\pm ($\in \mathcal{E}^\pm$) and the second sum excludes p_L ($\in \mathcal{N}^+$) and p_l^+ ($\in \mathcal{E}^+$). We rewrite this Hamiltonian as a spin-1/2 quantum Ising chain model interacting with an impurity spin-1/2 positioned at the chain's center, under the influence of a Zeeman field.

The spin chain is constructed from the plaquette centers (p) such that $p \in (-\infty, p_L] \cup [p_R, \infty)$. Then, we make the dimer \mathcal{H}_d^α part of the chain, placing it between p_L and p_R , and then label it by τ_0^α . In this way, a τ spin chain is obtained, which is coupled to the domino spin, τ_{dom} (which we referred to as the impurity spin). The Hamiltonian therefore becomes,

$$\begin{aligned} \tilde{H}^{(m)} = & \left[-h_z \sum_{i \notin \{-1, 0\}} \tau_i^x \tau_{i+1}^x - J \sum_{i \neq 0} \tau_i^z \right] - (\sqrt{2}J\tau_{\text{dom}}^z + h_z\tau_{\text{dom}}^x) \\ & - \frac{h_z}{2} \left[(\tau_{-1}^x \tau_0^x + \tau_0^x \tau_{+1}^x)(\tau_{\text{dom}}^x + \mathbf{1}) + (\tau_{-1}^x \tau_0^y - \tau_0^y \tau_{+1}^x)(\tau_{\text{dom}}^x - \mathbf{1}) \right], \end{aligned} \quad (\text{S32})$$

which is Eqs. (8)-(12) of the main text.

B. Field-induced dynamics of e anyons

We now consider the action of $-h_x \sum_{l \in r_e} \sigma_l^x$ on the zero-field XYJC. After the unitary rotation (of spins), $\sigma^x \rightarrow \sigma^y$, in the \mathcal{S} region (see Eq. (S18)). Therefore, the magnetic field also leads to fluctuations in the m sector. We replace $A_v^z \rightarrow \tau_v^z$ to denote the presence or absence of an e anyon. In the \mathcal{N} region, σ_l^x creates two e charges at the two ends of the horizontal link l (see Fig. S2),

$$-h_x \sum_{l \in r_e} \delta(l \in \mathcal{N}) \sigma_l^x = -h_x \sum_{\langle vv' \rangle \in \mathcal{N}} \tau_v^x \tau_{v'}^x, \quad (\text{S33})$$

where $\langle vv' \rangle \equiv l$ denotes the nearest-neighbor links of the lattice in the \mathcal{N} region that connect two vertices v and $v' = v + 1$. In the southern (\mathcal{S}^+) region, the σ^y field creates both e and m charges in pairs (see Fig. S2),

$$-h_x \sum_{l \in r_e} \delta(l \in \mathcal{S}^+) \sigma_l^y = -h_x \sum_{\substack{\langle v, v' \rangle \in \mathcal{S}^+ \\ \langle v, v' \rangle \perp \langle p, p' \rangle}} \tau_v^x \tau_{v'}^x \tau_p^x \tau_{p'}^x. \quad (\text{S34})$$

The m charges are created on the two plaquettes p, p' , that share the common link l .

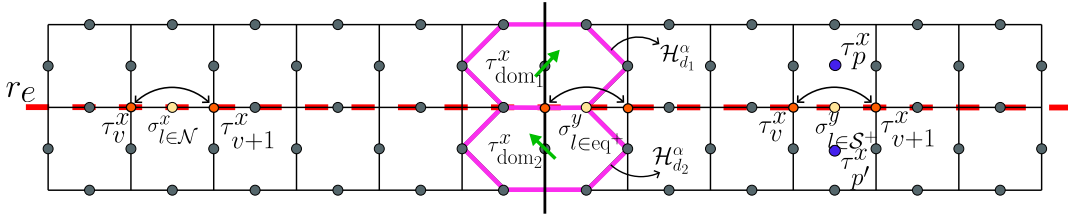


FIG. S2. Diagram illustrating various field-driven processes of e charge dynamics along the r_e string in the dual spin (τ) framework.

For the link $l = \text{eq}^+$, located directly to the right of the junction, the action of $\sigma_{\text{eq}^+}^y$ has several consequences (see Fig. S2), in addition to creating two e charges at its two ends. (i) The eigenvalues of the two dimer operators (H_{d_1} , H_{d_2}) that share the common link eq^+ , are flipped. (ii) The two domino operators D_{d_1} , and D_{d_2} , which also share the link eq^+ will transform to D'_{d_1} , and D'_{d_2} respectively. Hence, to evaluate the effective action of $\sigma_{\text{eq}^+}^y$, we must follow a similar procedure used to determine the action of σ^z across the junction (see the discussion in Sec. III A).

Consider the general eigenstate of the zero-field XYJC model in the z basis (Eq. (S19)) that has no e charges. Since σ_l^y creates two e charges at the ends of the link l , we create such a state from Eq. (S19), by flipping the spin at the eq^+ link of the reference state,

$$\begin{aligned} & \left\{ \{r_d^h\}_{d \in \mathcal{E}_q}, \{r_d\}_{d \in \mathcal{E}_q}, \{r_p\}_{p \in (\mathcal{N}^+, \mathcal{S}^+)}, r_1^v, r_2^v \right\} = \\ & \prod_{d \in \mathcal{E}_q} [1 + (-1)^{r_d^h} H_d] \left[1 + (-1)^{r_d} D_d \right] \prod_{p \in \mathcal{N}^+, \mathcal{S}^+} [1 + (-1)^{r_p} B_p^x] \left\{ |\downarrow\rangle_{\text{eq}^+} \bigotimes_{l \notin \text{eq}^+} |\uparrow\rangle_l^z \right\}. \end{aligned} \quad (\text{S35})$$

The (static) e anyons are placed in this state on the two nearest-neighbor vertices v_1 and v_2 connected by eq^+ . We consider the action of $\sigma_{\text{eq}^+}^y$ on the eigenstate Eq. (S19),

$$\begin{aligned} \sigma_{\text{eq}^+}^y \left| \{r_d^h\}_{d \in \mathcal{E}_q}, \{r_d\}_{d \in \mathcal{E}_q}, \{r_p\}_{p \in (\mathcal{N}^+, \mathcal{S}^+)} \right\rangle &= \prod_{i=1,2} (1 + (-1)^{r_{d_i}^h + 1} H_{d_i}) \prod_{\substack{d \in \mathcal{E}_q \\ d \neq d_1, d_2}} (1 + (-1)^{r_d^h} H_d) \\ &\times \prod_{i=1,2} (1 + (-1)^{r_{d_i}} D'_{d_i}) \prod_{\substack{d \in \mathcal{E}_q \\ d \neq d_1, d_2}} (1 + (-1)^{r_d} D_d) \prod_{p \in \mathcal{N}^+, \mathcal{S}^+} \left(1 + (-1)^{r_p} B_p^x \right) \left\{ \left| \downarrow \right\rangle_{\text{eq}^+} \otimes \left| \uparrow \right\rangle_e^z \right\}. \end{aligned} \quad (\text{S36})$$

To simplify the notation, we denote $\left| \{r_d^h\}_{d \in \mathcal{E}_q}, \{r_d\}_{d \in \mathcal{E}_q}, \{r_p\}_{p \in (\mathcal{N}^+, \mathcal{S}^+)} \right\rangle$ as $|r_{d_1}, r_{d_2}, r_{d_1}^h, r_{d_2}^h\rangle$ and $\left| \{r_d^h\}_{d \in \mathcal{E}_q}, \{r_d\}_{d \in \mathcal{E}_q}, \{r_p\}_{p \in (\mathcal{N}^+, \mathcal{S}^+)} \right\rangle$ as $|r_{d_1}, r_{d_2}, r_{d_1}^h, r_{d_2}^h, r_1^v, r_2^v\rangle$. We must have,

$$\sigma_{\text{eq}^+}^y |r_{d_1}, r_{d_2}, r_{d_1}^h, r_{d_2}^h\rangle = \sum_{p \in \mathcal{R}_D} c_p |r_{d_1}^h + 1, r_{d_2}^h + 1, r_1^v, r_2^v\rangle \otimes |p\rangle, \quad (\text{S37})$$

where the sum over p runs over the set: $\mathcal{R}_D = \{(r_{d_1}, r_{d_2}), (r_{d_1} + 1, r_{d_2}), (r_{d_1}, r_{d_2} + 1), (r_{d_1} + 1, r_{d_2} + 1)\}$ and c_p are appropriate coefficients. A straightforward calculation yields the following,

$$\begin{aligned} c_{(r_{d_1}, r_{d_2})} &= \prod_{i=1,2} \frac{1}{\sqrt{2}} \exp\left(i\frac{\pi}{4}(-1)^{r_{d_i}^h}\right), \quad c_{(r_{d_1}+1, r_{d_2})} = \frac{1}{\sqrt{2}} \exp\left(-i\frac{\pi}{4}(-1)^{r_{d_1}^h}\right) \times \frac{1}{\sqrt{2}} \exp\left(i\frac{\pi}{4}(-1)^{r_{d_2}^h}\right), \\ c_{(r_{d_1}, r_{d_2}+1)} &= \frac{1}{\sqrt{2}} \exp\left(i\frac{\pi}{4}(-1)^{r_{d_1}^h}\right) \times \frac{1}{\sqrt{2}} \exp\left(-i\frac{\pi}{4}(-1)^{r_{d_2}^h}\right) \quad \text{and} \quad c_{(r_{d_1}+1, r_{d_2}+1)} = \prod_{i=1,2} \frac{1}{\sqrt{2}} \exp\left(-i\frac{\pi}{4}(-1)^{r_{d_i}^h}\right). \end{aligned} \quad (\text{S38})$$

Hence, the action of $\sigma_{\text{eq}^+}^y$ is given by,

$$\begin{aligned} \sigma_{\text{eq}^+}^y &= \frac{1}{2} \tau_{v_1}^x \tau_{v_2}^x \mathcal{H}_{d_1}^x \mathcal{H}_{d_2}^x \left[e^{i\frac{\pi}{4}\mathcal{H}_{d_1}^z} e^{i\frac{\pi}{4}\mathcal{H}_{d_2}^z} \mathbb{1}_{\text{dom}_1} \otimes \mathbb{1}_{\text{dom}_2} + e^{-i\frac{\pi}{4}\mathcal{H}_{d_1}^z} e^{i\frac{\pi}{4}\mathcal{H}_{d_2}^z} \tau_{\text{dom}_1}^x \otimes \mathbb{1}_{\text{dom}_2} \right. \\ &\quad \left. + e^{i\frac{\pi}{4}\mathcal{H}_{d_1}^z} e^{-i\frac{\pi}{4}\mathcal{H}_{d_2}^z} \mathbb{1}_{\text{dom}_1} \otimes \tau_{\text{dom}_2}^x + e^{-i\frac{\pi}{4}\mathcal{H}_{d_1}^z} e^{-i\frac{\pi}{4}\mathcal{H}_{d_2}^z} \tau_{\text{dom}_1}^x \otimes \tau_{\text{dom}_2}^x \right]. \end{aligned} \quad (\text{S39})$$

Using the identity, $\mathcal{H}^x e^{\pm i\pi\mathcal{H}^z/4} = (\mathcal{H}^x \pm \mathcal{H}^y)/\sqrt{2}$, we can simplify the above as follows. We work in a rotated basis for the \mathcal{H}^α spins, $\tilde{\mathcal{H}}^x = (\mathcal{H}^x - \mathcal{H}^y)/\sqrt{2}$, $\tilde{\mathcal{H}}^y = (\mathcal{H}^x + \mathcal{H}^y)/\sqrt{2}$, $\tilde{\mathcal{H}}^z = \mathcal{H}^z$. The action of $\tilde{\mathcal{H}}^{x,y}$ on \mathcal{H}^z eigenstates are: $\tilde{\mathcal{H}}^x |\mathcal{H}^z = \pm 1\rangle = e^{\mp i\pi/4} |\mathcal{H}^z = \mp 1\rangle$, and $\tilde{\mathcal{H}}^y |\mathcal{H}^z = \pm 1\rangle = e^{\pm i\pi/4} |\mathcal{H}^z = \mp 1\rangle$. Thus, upto a phase factor, the actions of $\tilde{\mathcal{H}}^{x,y}$ are basically *spin-flip* operations. In terms of these new spin variables,

$$\sigma_{\text{eq}^+}^y = \frac{1}{2} \tau_{v_1}^x \tau_{v_2}^x \left[\tilde{\mathcal{H}}_{d_1}^y \tilde{\mathcal{H}}_{d_2}^y + \tilde{\mathcal{H}}_{d_1}^x \tilde{\mathcal{H}}_{d_2}^y \tau_{\text{dom}_1}^x + \tilde{\mathcal{H}}_{d_1}^y \tilde{\mathcal{H}}_{d_2}^x \tau_{\text{dom}_2}^x + \tilde{\mathcal{H}}_{d_1}^x \tilde{\mathcal{H}}_{d_2}^x \tau_{\text{dom}_1}^x \tau_{\text{dom}_2}^x \right]. \quad (\text{S40})$$

Thus, in the \mathcal{S} region, the action of the h_x Zeeman field has several consequences besides creating a pair of e charges (or hopping an e charge over a link): (1) near the junction, it flips a pair of \mathcal{H}^z and τ_{dom}^z spins, and (2) away from the junction (in the \mathcal{S}^+ region), it creates a pair of m excitations at plaquettes that share the common link l .

The Eqs. (S33), (S34), and (S40) describe the full action of the σ^x magnetic field for the e charge dynamics. Since J is always greater than h_x , the two domino spins ($\tau_{\text{dom}_1}, \tau_{\text{dom}_2}$) remain rigidly aligned along the $+z$ direction. This suppresses the last three terms in Eq. (S40), resulting in $\sigma_{\text{eq}^+}^y \approx \tau_{v_1}^x (\tilde{\mathcal{H}}_{d_1}^y \tilde{\mathcal{H}}_{d_2}^y) \tau_{v_2}^x$. Consequently, hopping an e anyon over the link eq^+ requires only two dimer flips which are energetically not as expensive as flipping domino spins (or creating m anyons). This is because there is no energy gap associated to dimer (H_d) fluctuations in the absence of Zeeman fields (and the gap is $\sim O(h_x)$ when the field is non-zero).

IV. Jordan-Wigner fermionization of the spin chain model describing m anyon dynamics in XY toric code junction

The spin chain Hamiltonian (Eq. (S32)), which describes the dynamics of m anyons along the chain r_m , can be mapped to a fermionic chain featuring both hopping and p -wave pairing terms, coupled to a spin- $\frac{1}{2}$ impurity at the

chain's center. This mapping is achieved through the Jordan-Wigner transformation [57], defined as follows:

$$\tau_i^x = \mathcal{S}_i(f_i + f_i^\dagger), \quad \tau_i^y = i\mathcal{S}_i(f_i^\dagger - f_i), \quad \tau_i^z = 1 - 2f_i^\dagger f_i, \quad \text{where } \mathcal{S}_i = \prod_{j<i} (1 - 2f_j^\dagger f_j). \quad (\text{S41})$$

The spin Hamiltonian (Eq. (S32)) transforms to,

$$\begin{aligned} \tilde{H}^{(m)} = & -h_z \sum_{i \notin \{-1,0\}} (f_i^\dagger f_{i+1}^\dagger + f_i^\dagger f_{i+1} + \text{H.c.}) - J \sum_{i \neq 0} (1 - 2n_i) - (\sqrt{2}J\tau_{\text{dom}}^z + h_z\tau_{\text{dom}}^x) \\ & - \frac{h_z}{2} \left[(1-i)f_{-1}^\dagger f_0^\dagger + (1+i)f_{-1}^\dagger f_0 + (1+i)f_0^\dagger f_1^\dagger + (1+i)f_0^\dagger f_1 + \text{H.c.} \right] \\ & - \frac{h_z}{2} \left[(1+i)f_{-1}^\dagger f_0^\dagger + (1-i)f_{-1}^\dagger f_0 + (1-i)f_0^\dagger f_1^\dagger + (1-i)f_0^\dagger f_1 + \text{H.c.} \right] \tau_{\text{dom}}^x. \end{aligned} \quad (\text{S42})$$

Using spinor operators $\Psi_i = (f_i, f_i^\dagger)^T$ in the particle-hole space, we can write the above Hamiltonian in a compact form,

$$\begin{aligned} \tilde{H}^{(m)} = & -\frac{1}{2} \sum_{i \notin \{-1,0\}} [\Psi_i^\dagger (t\tau^z + i\Delta\tau^y) \Psi_{i+1} + \text{H.c.}] - \frac{\mu}{2} \sum_{i \neq 0} \Psi_i^\dagger \tau^z \Psi_i - (\sqrt{2}J\tau_{\text{dom}}^z + h_z\tau_{\text{dom}}^x) \\ & - h_z (\Psi_{-1}^\dagger \tilde{\mathbf{B}}_{L,1}^\dagger \Psi_0 + \Psi_0^\dagger \tilde{\mathbf{B}}_{R,1}^\dagger \Psi_1 + \text{H.c.}) - h_z (\Psi_{-1}^\dagger \tilde{\mathbf{B}}_{L,2}^\dagger \Psi_0 + \Psi_0^\dagger \tilde{\mathbf{B}}_{R,2}^\dagger \Psi_1 + \text{H.c.}) \tau_{\text{dom}}^x, \end{aligned} \quad (\text{S43})$$

where $\mu = -2J$, and $t = \Delta = h_z$. The $\tilde{B}_{L/R,1/2}$ matrices are defined as follows,

$$\tilde{\mathbf{B}}_{L,1} = -\frac{1}{4} \begin{bmatrix} 1-i & -(1-i) \\ 1+i & -(1+i) \end{bmatrix}, \quad \tilde{\mathbf{B}}_{R,1} = -\frac{1}{4} \begin{bmatrix} 1-i & -(1+i) \\ 1-i & -(1+i) \end{bmatrix}, \quad (\text{S44})$$

and,

$$\tilde{\mathbf{B}}_{L,2} = -\frac{1}{4} \begin{bmatrix} 1+i & -(1+i) \\ 1-i & -(1-i) \end{bmatrix}, \quad \tilde{\mathbf{B}}_{R,2} = -\frac{1}{4} \begin{bmatrix} 1+i & -(1-i) \\ 1+i & -(1-i) \end{bmatrix}. \quad (\text{S45})$$

This form of the Hamiltonian is amenable to a transmission probability computation using the wave-function matching formalism described in the next section.

V. Wavefunction matching formalism for calculating transmission probability

Here, we describe the framework of the ‘‘wavefunction matching’’ approach [58] to compute m anyon transmission probability for the XY junction problem, governed by the Hamiltonian Eq. (S43). The same method is also used for the J_1 - J_2 junction problem. The key principle is the continuity of wavefunctions, which connects the states far from the scattering center (junction) to those near the scattering region. Leveraging this property, the infinite-dimensional time-independent Schrödinger equation for the entire system can be reduced to solving a finite set of linear inhomogeneous equations that capture the dynamics near the scattering center.

We first derive the ideal lead eigenstates, i.e., solutions in the absence of impurity or scatterer.

Ideal lead solutions: The Hamiltonian away from the impurity is simply the fermionic Kitaev chain model [68]. In the particle-hole space, the Hamiltonian matrix elements are given by,

$$H_{i,i+1} = \langle i | H | i+1 \rangle = \mathbf{B}_{L/R}^\dagger = -(t\tau^z + i\Delta\tau^y)/2, \quad H_{i,i} = \langle i | H | i \rangle = \mathbf{H}_{L/R} = -\mu\tau^z/2, \quad (\text{S46})$$

where $\mu = -2J$, $t = h$, $\Delta = h$ are the coupling parameters of the left (L) and right (R) leads. The left and right lead Hamiltonians do not couple to the domino spin (τ_{dom}^α) and therefore act as identity in the domino spin space.

The energy eigenvalue equation for the leads is given by,

$$-\mathbf{H}_{i,i-1}\Phi_{i-1} + (E - \mathbf{H}_{i,i})\Phi_i - \mathbf{H}_{i,i+1}\Phi_{i+1} = 0, \quad (\text{S47})$$

where $\mathbf{H}_{i,j}$ are the Hamiltonian blocks connecting the sites i and j . At every site, there is a 4 dimensional state space, which is a direct product of domino spin (dim=2) and particle-hole (dim=2) spaces,

$$\mathbf{H}_{i,i-1} = \mathbb{1}_{2 \times 2} \otimes (\mathbf{B}_{L/R})_{2 \times 2}, \quad \mathbf{H}_{i,i+1} = \mathbb{1}_{2 \times 2} \otimes (\mathbf{B}_{L/R}^\dagger)_{2 \times 2}, \quad \mathbf{H}_{i,i} = \mathbb{1}_{2 \times 2} \otimes (\mathbf{H}_{L/R})_{2 \times 2}. \quad (\text{S48})$$

Because of translation symmetry of the leads, the onsite and off-diagonal Hamiltonians are position-independent.

The lead modes have the following structure,

$$\Phi_i = \begin{pmatrix} c_+ \\ c_- \end{pmatrix} \otimes \Psi_i, \quad (\text{S49})$$

where c_\pm are arbitrary complex numbers representing the two spin components of the lead wavefunction. Since there is no coupling between the fermions and the domino spin inside the leads, the time-independent Schrodinger equation (Eq. (S47)) can be separated into spin and fermion parts, where the spin part is just the trivial identity operation and for the fermion part, one obtains the following

$$-\mathbf{B}_{L/R} \Psi_{i-1} + (E - \mathbf{H}_{L/R}) \Psi_i - \mathbf{B}_{L/R}^\dagger \Psi_{i+1} = 0. \quad (\text{S50})$$

According to Bloch's theorem, the wave functions at successive sites are related by a phase, and for a two-component wavefunction, it is a (uni-modular) matrix, i.e., $\Psi_i = F(\pm) \Psi_{i-1}$. Generalization of the usual Bloch phases ($e^{\pm ika}$) to the multi-orbital case ($n_{\text{orb}} = 2$) leads to the following Block matrix [58],

$$\mathbf{F}(\pm) = \sum_{n=1}^2 \lambda_{n,\pm} \mathbf{u}_n(\pm) \mathbf{u}_n^\dagger(\pm), \quad (\text{S51})$$

Here, $\lambda_{n,\pm} = e^{\pm ika}$ (independent of n), where n indexes the orbital. The value of k is related to energy E by the following identity,

$$\cos k = \frac{E^2 - (\mu/2)^2 - t^2}{2(\mu/2)t}. \quad (\text{S52})$$

The two column vectors $\mathbf{u}_1(\pm) = [\cos(\theta_k/2), \pm i \sin(\theta_k/2)]^T$ and $\mathbf{u}_2(\pm) = [\pm i \sin(\theta_k/2), \cos(\theta_k/2)]^T$ correspond to the particle- and hole-like normal modes of the time-independent Schrödinger equation, Eq.(S50). The \pm denotes the chirality of these states (right or left moving nature). The Bloch matrix is determined from explicit evaluation of Eq. (S51), and is proportional to identity,

$$\mathbf{F}(\pm) = e^{\pm ika} \mathbb{1}_{2 \times 2}, \quad (\text{S53})$$

The general (propagating wave) solution of the Bloch equation is given by,

$$\Psi_i = \mathbf{F}^{i-j}(+) \Psi_j(+) + \mathbf{F}^{i-j}(-) \Psi_j(-), \quad (\text{S54})$$

where $\mathbf{F}^m(\pm) = \sum_{n=1}^2 (\lambda_{n,\pm})^m \mathbf{u}_n(\pm) \mathbf{u}_n^\dagger(\pm) = e^{\pm imka} \mathbb{1}_{2 \times 2}$, for any integer m .

Wavefunction matching: By matching the states near the scatterer with the traveling Bloch wave solutions, we can derive equations for Ψ_{-1} and Ψ_{S+2} (wavefunction amplitudes near the scattering region), where S = the size of the scattering region. This helps us to truncate the infinite-dimensional Schrodinger equation (of the full problem) to a $(S + 2)$ dimensional matrix equation. For the Hamiltonian Eq. (S42), $S = 1$ (for the single impurity), while for the J_1 - J_2 model, $S = W$ (the width of the J_2 region). The wavefunction amplitude at $i = -1$ (which is within the left lead) can be obtained from the general solution, Eq. (S54),

$$\Psi_{-1} = \mathbf{F}_L^{-1}(+) \Psi_0(+) + \mathbf{F}_L^{-1}(-) \Psi_0(-). \quad (\text{S55})$$

We substitute $\Psi_0(-) = \Psi_0 - \Psi_0(+)$ (also obtained from Eq. (S54)) in the above equation to obtain,

$$\Psi_{-1} = (\mathbf{F}_L^{-1}(+) - \mathbf{F}_L^{-1}(-)) \Psi_0(+) + \mathbf{F}_L^{-1}(-) \Psi_0. \quad (\text{S56})$$

The time-independent Schrodinger equation (Eq. (S47)) at $i = 0$, which is at the boundary between the scattering region ($i = 1, \dots, S$) and the left lead ($i = -\infty, \dots, -1, 0$), is given by,

$$-\mathbf{H}_{0,-1} \Phi_{-1} + (E - \mathbf{H}_{0,0}) \Phi_0 - \mathbf{H}_{0,1} \Phi_1 = 0. \quad (\text{S57})$$

From Eq. (S48), $\mathbf{H}_{0,-1} = \mathbf{1}_s \otimes (\mathbf{B}_L)$, and $\mathbf{H}_{0,0} = \mathbf{H}_L$. On the other hand, $\mathbf{H}_{0,1} = \mathbf{1} \otimes \tilde{\mathbf{B}}_{L,1}^\dagger + \tau^x \otimes \tilde{\mathbf{B}}_{L,2}^\dagger$ (hopping matrices connecting the left lead and the site $i = 1$ (the impurity site)). Replace Ψ_{-1} in Eq. (S57) by Eq. (S56), to obtain the following,

$$[\mathbf{1} \otimes (E - \mathbf{H}_L - \mathbf{B}_L \mathbf{F}_L^{-1}(-))] \Phi_0 - [\mathbf{1} \otimes \tilde{\mathbf{B}}_{L,1}^\dagger + \tau^x \otimes \tilde{\mathbf{B}}_{L,2}^\dagger] \Phi_1 = [\mathbf{1} \otimes \mathbf{B}_L (\mathbf{F}_L^{-1}(+) - \mathbf{F}_L^{-1}(-))] \Phi_0(+), \quad (\text{S58})$$

where $\Phi_0(+)$ is the amplitude at site $i = 0$ of the incoming (right-moving) wave coming from the left lead,

$$\Phi_0(+) = \mathbf{u}_\sigma^s \otimes \mathbf{u}_{L,m}^f(+); \quad \sigma = \uparrow, \downarrow, m = 1, 2, \quad (\text{S59})$$

and $\mathbf{u}_\sigma^s = \{(1, 0)^\text{T}, (0, 1)^\text{T}\}$ are the two possible eigenstates of τ_{dom}^z . The states $\mathbf{u}_{L,m}^f(+)$ are the right-moving eigenmodes of the left lead.

For $i = S + 1$, which is at the boundary between the scattering region ($i = 1, \dots, S$) and the right lead ($i = (S + 1), \dots, +\infty$), the time-independent Schrodinger equation is given by,

$$-[\mathbf{1} \otimes \tilde{\mathbf{B}}_{R,1} + \tau^x \otimes \tilde{\mathbf{B}}_{R,2}] \Phi_S + [\mathbf{1} \otimes (E - \mathbf{H}_R)] \Phi_{S+1} - [\mathbf{1} \otimes \mathbf{B}_R^\dagger] \Phi_{S+2} = 0. \quad (\text{S60})$$

There is no left-moving wave from the right lead; $\Psi_{S+1}(-) = 0$. Therefore, $\Psi_{S+2} = \mathbf{F}_R(+)\Psi_{S+1}$. Substituting this in the Schrodinger equation, one obtains,

$$-[\mathbf{1} \otimes \tilde{\mathbf{B}}_{R,1} + \tau^x \otimes \tilde{\mathbf{B}}_{R,2}] \Phi_S + [\mathbf{1} \otimes (E - \mathbf{H}_R - \mathbf{B}_R^\dagger \mathbf{F}_R(+))] \Phi_{S+1} = 0. \quad (\text{S61})$$

The time-independent Schrodinger equation at the scattering center ($i = S = 1$) is given by,

$$-\mathbf{H}_{1,0} \Phi_0 + (E - \mathbf{H}_{1,1}) \Phi - \mathbf{H}_{1,2} \Phi_2 = 0. \quad (\text{S62})$$

Here, $\mathbf{H}_{1,0} = \mathbf{1} \otimes \tilde{\mathbf{B}}_{L,1} + \tau^x \otimes \tilde{\mathbf{B}}_{L,2}$, $\mathbf{H}_{1,2} = \mathbf{1} \otimes \tilde{\mathbf{B}}_{R,1}^\dagger + \tau^x \otimes \tilde{\mathbf{B}}_{R,2}^\dagger$, and $\mathbf{H}_{1,1} = \mathbf{H}_0$ is the impurity Hamiltonian, which is given by $\mathbf{H}_0 = -(\sqrt{2}J\tau^z + h_z\tau^x) \otimes \mathbf{1}_f$.

The lead self-energies are given by the following expressions,

$$\Sigma_L = \mathbf{B}_L \mathbf{F}_L^{-1}(-) = -\frac{t}{2} e^{ik} (\tau^z - i\tau^y), \quad (\text{S63})$$

$$\Sigma_R = \mathbf{B}_R^\dagger \mathbf{F}_R(+)= -\frac{t}{2} e^{ik} (\tau^z + i\tau^y). \quad (\text{S64})$$

The Eqs. (S58), (S61), (S62) can be combined to a compact matrix form,

$$E - \mathbf{H}' = \begin{bmatrix} \mathbf{1}_s \otimes (E - \mathbf{H}_L - \Sigma_L) & -(\mathbf{1}_s \otimes \tilde{\mathbf{B}}_{L,1}^\dagger + \tau^x \otimes \tilde{\mathbf{B}}_{L,2}^\dagger) & 0 \\ -(\mathbf{1}_s \otimes \tilde{\mathbf{B}}_{L,1} + \tau^x \otimes \tilde{\mathbf{B}}_{L,2}) & (E + \sqrt{2}J\tau^z + h_z\tau^x) \otimes \mathbf{1}_f & -(\mathbf{1}_s \otimes \tilde{\mathbf{B}}_{R,1}^\dagger + \tau^x \otimes \tilde{\mathbf{B}}_{R,2}^\dagger) \\ 0 & -(\mathbf{1} \otimes \tilde{\mathbf{B}}_{R,1} + \tau^x \otimes \tilde{\mathbf{B}}_{R,2}) & \mathbf{1}_s \otimes (E - \mathbf{H}_R - \Sigma_R), \end{bmatrix} \quad (\text{S65})$$

and,

$$(E - \mathbf{H}') \begin{bmatrix} \Phi_0 \\ \Phi_1 \\ \Phi_2 \end{bmatrix} = \begin{bmatrix} \mathbf{Q}_0 \\ 0 \\ 0 \end{bmatrix}, \quad (\text{S66})$$

where

$$\mathbf{Q}_0 = (\mathbf{1}_s \otimes \mathbf{B}_L [\mathbf{F}_L^{-1}(+) - \mathbf{F}_L^{-1}(-)]) \Phi_0(+). \quad (\text{S67})$$

For the J_1 - J_2 model, there is no impurity (domino) spin. The block matrix \mathbf{H}' has size $2(S + 2) \times 2(S + 2)$, where $S = W$ (the width of the J_2 region) and the factor 2 comes from the particle and hole orbitals.

Transmission probability calculation: From the solution of $(E - H')\psi = \mathbf{Q}$, the transmitted wave amplitude Φ_2 can be obtained, which is a direct product of spin and orbital wavefunctions,

$$\Phi_2 = \begin{pmatrix} a_+ \\ a_- \end{pmatrix} \otimes \Psi_2. \quad (\text{S68})$$

We expand the right-moving transmitted wave (Φ_2) in the eigenbasis of the right leads,

$$\Phi_2^{(m,\sigma')} = \sum_{n=1}^2 \sum_{\sigma=\uparrow,\downarrow} \mathbf{u}_\sigma^s \otimes \mathbf{u}_{R,n}^f(+)\ t_{n\sigma,m\sigma'}, \quad (\text{S69})$$

where \mathbf{u}_σ^s and $\mathbf{u}_{R,n}^f$ correspond to spin and (right-moving) Bogoliubov fermion wavefunctions respectively. The coefficients are the elements of the transmission matrix which are obtained as follows,

$$t_{n\sigma,m\sigma'} = [\mathbf{u}_\sigma^s \otimes \mathbf{u}_{R,n}^f(+)]^\dagger \Phi_2^{(m,\sigma')}. \quad (\text{S70})$$

After calculating the (4×4) transmission matrix (\mathbf{t}), we can obtain the transmission probability (T) by taking the trace,

$$T(E) = \frac{1}{4} \text{Tr}(\mathbf{t}\mathbf{t}^\dagger), \quad (\text{S71})$$

The $1/4$ factor is for normalization (two factors of $1/2$ account for averaging over the spin and particle-hole spaces, respectively).

VI. Continuum description of $\tilde{H}^{(m)}$

In this section, we derive the effective low-energy theory for the lattice model (Eq. (S43)) that describes the motion of m anyons across the XY junction. To derive that, we divide the Hamiltonian into four parts, $\tilde{H}^{(m)} = H_f^{(0)} + H_{\text{dom}} + V_f + V_{fs}$, where $H_f^{(0)}$ is the uniform Kitaev chain Hamiltonian,

$$H_f^{(0)} = -h_z \sum_i (f_i^\dagger f_{i+1}^\dagger + f_i^\dagger f_{i+1} + h.c.) - J \sum_i (1 - 2n_i), \quad (\text{S72})$$

and H_{dom} governs the spin dynamics of the domino spin,

$$H_{\text{dom}} = -\sqrt{2}J\tau_{\text{dom}}^z - h_z\tau_{\text{dom}}^x. \quad (\text{S73})$$

There is a perturbation in the hopping and pairing, acting on the bonds adjacent to the junction (or the site $i = 0$), and also an onsite potential at $i = 0$,

$$V_f = \frac{h_z}{2} \left[(1+i)f_{-1}^\dagger f_0^\dagger + (1-i)f_{-1}^\dagger f_0 + (1-i)f_0^\dagger f_1^\dagger + (1-i)f_0^\dagger f_1 + \text{H.c.} \right] + J(1 - 2f_0^\dagger f_0). \quad (\text{S74})$$

The domino spin and the fermions are coupled by,

$$V_{fs} = -\frac{h_z}{2} \left[(1+i)f_{-1}^\dagger f_0^\dagger + (1-i)f_{-1}^\dagger f_0 + (1-i)f_0^\dagger f_1^\dagger + (1-i)f_0^\dagger f_1 + \text{H.c.} \right] \tau_{\text{dom}}^x. \quad (\text{S75})$$

The first step in taking the continuum approximation involves finding the low-energy modes of the unperturbed system (Eq. (S72)). In this case, these are the $k \sim 0$ Bogoliubov excitations above $\Delta = 2(J - h_z)$. Near $k = 0$, and when $h_z < J$, $u_{k \sim 0} = 0$ and $v_{k \sim 0} = 1$ (upto a \mathbb{Z}_2 phase). Therefore, from the relation $f_k = u_k \gamma_k - i v_k \gamma_{-k}^\dagger$, one obtains $\frac{1}{\sqrt{N}} \sum_{k \sim 0} f_k e^{-ikx_i} = -\frac{i}{\sqrt{N}} \sum_{k \sim 0} \gamma_k^\dagger e^{ikx_i}$. This implies $\tilde{f}_i = -i\tilde{\gamma}_i^\dagger$, where we put tilde on the operators to distinguish their $k \sim 0$ (soft) mode from the lattice fermion operators. The latter also involve rapidly oscillating parts, $f_i = \tilde{f}_i + \frac{1}{\sqrt{N}} \sum_{|k| > \Lambda_0} f_k e^{-ikx_i}$, where Λ_0 is the cut-off beyond which the energy dispersion of $H_f^{(0)}$ is no longer quadratic. In the long-wavelength limit, we can safely ignore such large-momentum contributions (beyond Λ_0). Thus, the low-energy Bogoliubov modes are *hole-like* excitations in our regime of interest.

Next, we normalize the lattice operators to get the continuum field operators,

$$\psi(x_i) = \frac{1}{\sqrt{a_0}} \tilde{\gamma}_i. \quad (\text{S76})$$

The non-interacting Kitaev chain Hamiltonian (Eq. (S72)) can be approximated as follows,

$$H_f^{(0)} = - \int dx \psi^\dagger(x) \left(\Delta_m + \frac{\partial_x^2}{2M_m} \right) \psi(x), \quad (\text{S77})$$

where $\tilde{J} = Ja_0$, $\tilde{h}_z = h_z a_0$ are the effective coupling strengths that survive in the continuum limit ($J, h_z \rightarrow \infty$, $a_0 \rightarrow 0$). The mass gap and the band mass of the quasiparticle are given by $\Delta_m = 2Ja_0(1-h/J)$ and $M_m = \Delta_m/4\tilde{h}_z\tilde{J}$.

Next, we find what happens to V_f in the continuum limit:

$$\begin{aligned} h_z [(1-i)f_0^\dagger f_1^\dagger - (1+i)f_0^\dagger f_{-1}^\dagger] &\approx h_z [-(1-i)\gamma_0\gamma_1 + (1+i)\gamma_0\gamma_{-1}] \quad (\text{ignoring the finite-}k \text{ contributions}) \\ &= -\tilde{h}_z [(1-i)\psi(x=0)\psi(x=a_0) - (1+i)\psi(x=0)\psi(x=-a_0)] \\ &\approx -2a_0\tilde{h}_z\psi(x)\partial_x\psi(x)|_{x=0} + \mathcal{O}(a_0^2). \end{aligned} \quad (\text{S78})$$

Since there is no sum over lattice sites, this term vanishes in the continuum limit, $a_0 \rightarrow 0$. For the hopping part, a finite contribution remains,

$$\begin{aligned} h_z [(1-i)f_{-1}^\dagger f_0 + (1-i)f_0^\dagger f_1 + h.c.] &\approx \tilde{h}_z [(1-i)\psi(-a_0)\psi^\dagger(0) + (1-i)\psi(0)\psi^\dagger(a_0) + \text{H.c.}] \\ &\approx -4\tilde{h}_z\psi^\dagger(0)\psi(0) - 2ia_0\tilde{h}_z \left[\psi^\dagger\partial_x\psi - (\partial_x\psi^\dagger)\psi \right]_{x=0} + \mathcal{O}(a_0^2). \end{aligned} \quad (\text{S79})$$

Only the first term survives in the limit $a_0 \rightarrow 0$ and therefore we obtain,

$$V_f \approx \Delta_m \psi^\dagger(x=0)\psi(x=0), \quad (\text{S80})$$

and V_{f_s} simplifies to the following expression,

$$V_{f_s} = \eta h_z \psi^\dagger(0)\psi(0)\tau_{\text{dom}}^x, \quad (\text{S81})$$

where η is a non-universal cut-off (Λ_0) dependent factor. Combining all these pieces, we obtain,

$$H^{(m)} = - \int dx \psi^\dagger(x) \left[\Delta_m(x) + \frac{\partial_x^2}{2M_m} \right] \psi(x) - \sqrt{2}J\tau_{\text{dom}}^z - h_z\tau_{\text{dom}}^x + \eta h_z \psi^\dagger(0)\psi(0)\tau_{\text{dom}}^x, \quad (\text{S82})$$

where $\Delta_m(x) = \Delta_m[1 - \delta(x)]$ is the inhomogeneous mass gap of the Bogoliubov soft modes (ψ). Note that these excitations face a Dirac delta barrier at the origin ($x = 0$) and the barrier strength depends on the combination $\Delta_m + \eta h_z \langle \tau_{\text{dom}}^x \rangle$, which depends on the ratio h_z/J . At the level of a mean-field approximation, $\langle \tau_{\text{dom}}^x \rangle = \tilde{h}_z / \sqrt{\tilde{h}_z^2 + 2J^2}$, where $\tilde{h}_z = h_z(1 - 2\langle \gamma_0^\dagger \gamma_0 \rangle)$. Now, $\langle \gamma_0^\dagger \gamma_0 \rangle = 1 - \langle f_0^\dagger f_0 \rangle$. When $h_z \sim 0$, there is no onsite energy term for $n_{i=0}^f$ and the hopping that connects $i = 0$ to the rest of the chain is only of $O(h_z)$, therefore negligible. So, we expect $\langle f_0^\dagger f_0 \rangle_{h \rightarrow 0} \approx 1/2$. For $i \neq 0$, $\langle f_i^\dagger f_i \rangle_{h \rightarrow 0} \approx 0$, because the onsite potential is positive (see Eq. (S72)). Naturally, when h_z becomes nonzero (but still small), $\langle f_0^\dagger f_0 \rangle < 1/2$, due to hopping between site $i = 0$ and the rest of the system. As a result, $\langle \tau_{\text{dom}}^x \rangle$ switches to a negative number. This is also confirmed in our m anyon wavepacket dynamics calculation (see Fig. (3) of the main text) of the lattice model Eq. (S43). As shown in Fig. S3, the domino spin remains rigidly aligned along the z direction, but once the m anyon hits the junction (around $Jt \approx 400$), $\langle \tau_{\text{dom}}^x \rangle$ becomes negative. The height of the delta barrier therefore decreases due to the combined effect of (i) reduction in onsite energy (Δ_m) at $i = 0$ and (ii) because $\langle \tau_{\text{dom}}^x \rangle$ becomes negative as h_z increases.

VII. Mapping e anyon dynamics to a 1d Z_2 gauge theory

While the e particle can move freely within the \mathcal{N} region, its behavior becomes complicated upon entering the \mathcal{S} region. Initially, right next to the junction, the hopping of the e charge induces quantum fluctuations in the dimer (H_d) and domino (τ_{dom}^x) sectors (see Eq. (S40)). Quantum fluctuations in the domino sector are suppressed if $h_x < J$. In the XYJC model, dimer spins can flip freely since these excitations are energetically degenerate in the zero-field limit, resulting in an almost negligible energy cost for flipping a dimer. Hence, the e charge can hop easily by flipping a dimer pair and cross the \mathcal{E}^+ region (see Fig. (3) of the main text). Across the \mathcal{S}^+ region, the e charge hopping generates pair fluctuations in the m sector. We will focus solely on the effects of m charge pairs on the dynamics of an e particle, as this process occurs throughout the \mathcal{S}^+ region, leading to a significant influence on the transport properties of the e particle.

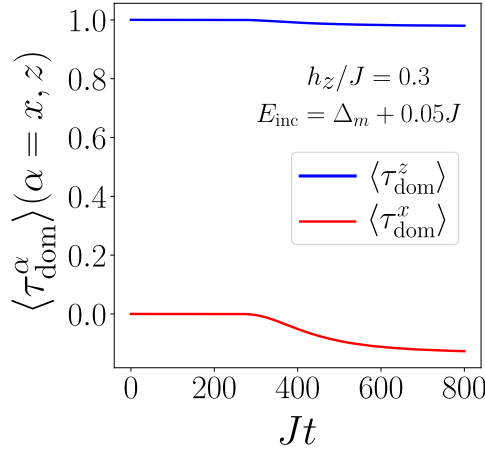


FIG. S3. Time evolution of the expectation values of domino spin components ($\langle \tau_{\text{dom}}^\alpha \rangle(t)$, for $\alpha = x, z$). The numerical data is for incident m anyon energy, $E_{\text{inc}} = \Delta_m + 0.05J$, and magnetic field strength, $h_z/J = 0.3$. The m anyon wave packet evolution is shown in the main text (see Fig.(3)) for the same data points.

Consider the part of the effective spin Hamiltonian that describes e charge dynamics in the \mathcal{S}^+ region,

$$H_{\mathcal{S}^+}^{(e)} = -J \sum_{v \in r_e} \tau_v^z - J \sum_{v \in r_e, \sigma = \pm} \tau_{v+1/2, \sigma}^z - h_x \sum_{v \in r_e} \tau_v^x (\tau_{v+1/2, +}^x \tau_{v+1/2, -}^x) \tau_{v+1}^x. \quad (\text{S83})$$

Here, v denotes the location of the A_v^z operators (or the static e anyon excitations) and $(v + 1/2, \pm)$ denote the two plaquette centers that share a common link $(v, v + 1) \in r_e$. This Hamiltonian describes the motion of gapped e anyon excitations in the vacuum of m charges, where their movement induces pair fluctuations of the m particles. We disregard the h_z coupling, which induces fluctuations solely in the m sector, and focus on examining the action of the h_x Zeeman field on the otherwise stationary e and m anyons. Conclusions obtained from this approximation will also remain valid when h_z is finite but $h_z < J$ (so that the m anyon gap $\sim (J - h_z)$ remains finite).

The h_x field creates m charges in pairs, at the plaquette centers labeled by $(v + 1/2, \pm)$. Thus, the $h_z = 0$ low-energy subspace for a given bond along the ladder rung is two-dimensional and comprises the states,

$$|\uparrow\rangle = |\tau_{v+\frac{1}{2}, +}^z = +1\rangle \otimes |\tau_{v+\frac{1}{2}, -}^z = +1\rangle, \quad |\downarrow\rangle = |\tau_{v+\frac{1}{2}, +}^z = -1\rangle \otimes |\tau_{v+\frac{1}{2}, -}^z = -1\rangle. \quad (\text{S84})$$

Consider the following operators defined on the bonds $(v, v + 1) \in r_e$,

$$X_{v, v+1} = \frac{1}{2} \left(\tau_{v+\frac{1}{2}, +}^z + \tau_{v+\frac{1}{2}, -}^z \right), \quad Z_{v, v+1} = \tau_{v+\frac{1}{2}, +}^x \tau_{v+\frac{1}{2}, -}^x. \quad (\text{S85})$$

These operators behave as Pauli spins within the low-energy subspace of $|\uparrow\rangle$ and $|\downarrow\rangle$, i.e., $(X_{vv'})^2 = 1 = (Z_{vv'})^2$ and $[Z_{vv'}, X_{vv'}]_+ = 0$ (where $v' = v + 1$). In terms of these *bond-spins*, our Hamiltonian becomes a 1d \mathbb{Z}_2 gauge theory,

$$H_{\mathcal{S}^+}^{(e)} = -J \sum_v \tau_v^z - 2J \sum_v X_{v, v+1} - h_x \sum_v \tau_v^x Z_{v, v+1} \tau_{v+1}^x. \quad (\text{S86})$$

The operator, $G_v = X_{v-1, v} \tau_v^z X_{v, v+1}$ is a symmetry of the above Hamiltonian. The bond-spins (and site-spins) correspond to the \mathbb{Z}_2 gauge fields (and \mathbb{Z}_2 matter fields) of the gauge theory. Restricting ourselves to a specific symmetry sector is equivalent to imposing the Gauss law constraint. The zero field sector corresponds to $G_v = +1 \forall v$ (finite h_x cannot change the symmetry sector).

One-dimensional gauge theories with matter show confinement. The gauge field string connecting two matter (e) charges will cost an energy that scales as the length of the string (or the separation between two e charges). The same is also true for a single e charge motion. The string tension thus grows as $\sim 4Jl$ (l = length of the string).

Thus, the e particle's motion in the \mathcal{S}^+ region is similar to that of a quantum particle under the influence of a linearly increasing potential, $V(x) = 0$, for $x < 0$, and $V(x) = \lambda x$, for $x \geq 0$. This leads to negligible transmission and significant reflection back into the \mathcal{N} region, when $h_x < J$. This explains the large opacity of the XYJC to the e -charge.